CEBAF Program Advisory Committee Six (PAC6) Proposal Cover Sheet

This proposal must be received by close of business on April 5, 1993 at:

CEBAF

User Liaison Office

12000 Jefferson Avenue

Newport News, VA 23606

Proposal Title

Measurement of the Structure Functions
for Kaon Electroproduction

Contact Person

Name: Mac Mestayer

Institution: CEBAF

Address: 12000 Jefferson Avenue

Address: Physics Division, MS12H

City, State ZIP/Country: Newport News, VA 23606

Phone: (804) 249-7252 **FAX:** (804)249-5800

E-Mail → BITnet: Mestayer@CEBAF **Internet:**

If this proposal is based on a previously submitted proposal or letter-of-intent, give the number, title and date:

Measurement of the Structure Functions for Kaon Electroproduction

Spokespersons:
M.D. Mestayer[1] and K.H. Hicks[2]

Participants:
T. Adami[2*], D. Doughty[1], S. Dytman[3], R.W. Finlay[2], H. Funsten[7], S. Grimes[2], R. Magahiz,[4],J. Rapaport[2],P. Rubin[7], R. Schumacher[4], E.S. Smith[1], and C.L. Tam[5]

Theoretical support:
C. Bennhold[6], S. Capstick[1], A. Kumar[2*], D.S. Onley[2], and L.E. Wright[2]

[1]Physics Division, CEBAF, Newport News, VA

[2]Department of Physics, Ohio University, Athens, OH

[3]Department of Physics, University of Pittsburgh, Pittsburgh, PA

[4]Department of Physics, Carnegie-Mellon University, Pittsburgh, PA

[5]Department of Physics, University of South Carolina, Columbia, SC

[6]Department of Physics, George Washington University, Washington, DC

[7]Department of Physics, College of William and Mary, Williamsburg, VA

*graduate student

Abstract

We propose to measure the four structure functions which describe kaon hyperon electroproduction over the Q^2 range from 1.0 to 2.5 GeV^2 and W from threshold (1.62 GeV) to 2.2 GeV. This region of Q^2 and W is a transition region where it is expected that a formalism based upon hadron dynamics (QHD) will become more economically expressed in terms of a quark description. The goal of the experiment is to obtain as comprehensive a data set as possible; measuring all four structure functions over a large range of Q^2, W, and t. This is made possible by the unique capabilities of the CLAS detector, which allows detection of the K^+ over practically the entire solid angle. The best way to constrain QHD models is by comparing them to as wide a range of observables as possible.

We explicitly mention six items of physical interest which this experiment will address:

1. measure the L,T,LT, and TT structure functions over a wide kinematic range,

2. measure the isospin dependence of the L/T ratio by comparing L/T for recoiling Λ versus Σ,

3. measure the t dependence of σ_L which is sensitive to the kaon form factor,

4. measure the production ratio of the various hyperons, Λ, Σ, $\Lambda(1405)$, $\Sigma(1385)$, and $\Lambda(1520)$ as a function of Q^2,

5. study the polarization of the produced $s\bar{s}$ pair by measuring the polarization of the Λ, and

6. search for missing N* resonances which decay to K^+-hyperon final states.

1   Scientific Motivation

The electroproduction of kaons is a rich topic, and the data can be used to test theoretical models in either a standard nucleon-meson picture or in a quark-model formulation. At present, very little data exist for this reaction, mainly due to the higher energies needed to create two strange particles. The old data [1], [2], [3], taken at DESY and Cornell in the 1970's, covered only a small portion of phase space and have fairly large statistical errors. At Cornell, they used a two-spectrometer system and had a limited amount of luminosity. The LAME detector [4] did exclusive electroproduction experiments including K^+ final states, but had limited particle identification capability and concentrated on $N\pi$ and $\Delta\pi$ final states. The CLAS detector at CEBAF is ideally suited to carry out these studies over a wide range of kinematics in a modest amount of beam-time. Its superconducting toroidal magnet affords nearly 4π solid angle coverage while allowing efficient running up to a luminosity of $10^{34}\text{cm}^{-2}\text{s}^{-1}$. The detector and tracking system are described in more detail in a recent NIM article[5].

Theoretical calculations in standard hadrodynamic models (QHD) are presently available for kaon electroproduction[6, 7]. Calculations in a simplified non-relativistic quark model (NRQM) have been developed for kaon photoproduction[8] and are being extended to electroproduction. The data proposed here, for the ^{1}H$(e,e'K^+)$ reaction, will explore whether the data is better described using nucleon/meson or quark degrees of freedom. The advantage of the NRQM is that it has fewer free parameters, since the photon is assumed to couple directly to the constituent quark, and thereby avoids the large number of coupling constants for each new resonance used in the QHD models.

The QHD and NRQM calculations can also be compared with the proposed kaon photoproduction measurements[9] to be done with CLAS. Some of the theoretical issues, such as the coupling constants mentioned above, will be constrained by these real-photon data ($Q^2 = 0$) where only transverse photon polarizations are considered. For the electroproduction data the longitudinal polarization of the photon will also contribute. We will perform a Rosenbluth separation and measure the ϕ dependence in the hadronic system to determine the four structure functions σ_T, σ_L, σ_{TT} and σ_{TL} over a range of Q^2. Especially interesting is the ratio of the longitudinal/transverse cross sections (L/T), which may be sensitive to dynamics beyond the physics in either the QHD model or the NRQM. The proposed measurements reach into unexplored kinematic territory, which could hold some interesting surprises. Even if no surprises are found in the L/T ratio, the ^{1}H$(e,e'K^+)$ data proposed here will complement the photoproduction data and further constrain models of the kaon form factor and the dynamics of the reaction mechanism.

3

1.1 Rosenbluth decomposition

The general form of the $(e, e'X)$ cross section is well known [10, 11] and consists of four components:

$$\frac{d\sigma}{d\Omega} = \sigma_T + \epsilon\sigma_{TT} \cos2\phi + \epsilon\sigma_L + \sqrt{\epsilon(\epsilon+1)/2} \; \sigma_{LT} \cos\phi \qquad (1)$$

where ϕ is the angle between the electron reaction plane and the photon-kaon reaction plane as shown in figure 1. Each of the four terms are functions of the kaon center of mass angle θ (with respect to the virtual photon direction), the 4-momentum transfer from the electron Q^2, and the total energy in the photon-proton system, W. The polarization parameter is given by

$$\epsilon = 1/[1 + 2(1 + \nu^2/Q^2)\tan^2(\theta_e/2)] \qquad (2)$$

where ν is the lab energy transfer from the electron.

The σ_T and σ_{TT} terms are respectively the sum and difference of the two transverse polarization states, given by [11]

$$\sigma_T = (\sigma_\| + \sigma_\perp)/2$$

and

$$\sigma_{TT} = (\sigma_\| - \sigma_\perp)/2$$

where only σ_T is measured with unpolarized photons. An over-all decomposition into the four terms is accomplished by measuring the cross section at points with the same value of Q^2 and W but at different beam energies, and hence, ϵ , while fitting to the observed ϕ dependence.

The photoproduction data is limited to measuring only the σ_T term, and if polarized, the σ_{TT} term, and only at $Q^2 = 0$. The advantage of the electroproduction data becomes apparent, especially with a detector such as CLAS. For electroproduction, the interference terms are multiplied by cosϕ or by cos2ϕ, and a conventional two-spectrometer measurement with limited out-of-plane capability will either average over ϕ if set up for parallel kinematics or can measure near $\phi = 180°$ for large values of t. In contrast, the CLAS detector will have virtually full coverage of the ϕ, θ range. High-statistics data from these four structure functions will severely constrain the reaction models.

1.2 Theoretical Calculations

1.2.1 The hadrodynamic model

Two models of kaon electroproduction using the standard picture of nucleons (and nucleon resonances) and mesons (and meson resonances) have been published in recent years by Adelseck, Bennhold and Wright (ABW) [6] and by Williams, Ji, and Cotanch (WJC) [7]. The diagrams used in these calculations are shown in figure 2 and the coupling constants, as determined by fits to existing photoproduction data, are given

4

Table 1: Coupling constants in the QHD model of reference [6], with errors as obtained from least squares analysis using the MINUIT code.

Coupling	Value
$g_{K\Lambda N}/\sqrt{4\pi}$	-4.17 ± 0.75
$g_{K\Sigma N}/\sqrt{4\pi}$	$+1.18 \pm 0.66$
$G_V/\sqrt{4\pi}$	-0.43 ± 0.07
$G_T/\sqrt{4\pi}$	$+0.20 \pm 0.12$
$G_{N1}/\sqrt{4\pi}$	-1.41 ± 0.60
$G_{Y3}/\sqrt{4\pi}$	-3.17 ± 0.86
$G_V^{K1}/\sqrt{4\pi}$	-0.10 ± 0.06
$G_T^{K1}/\sqrt{4\pi}$	-1.21 ± 0.33

in Table 1 in the ABW model. These diagrams can be broken down into s, u, and t exchange. The importance of including the K^* resonance in the t-channel is shown in figure 3, from the WJC model. In both the WJC and the ABW models, good agreement is obtained with the limited data by fitting the coupling constants (or other parameters) that are not already constrained.

There are two main criticisms to these models. One is the large number of coupling constants, which appear in each new diagram of the calculation. Even beyond this, questions of duality[7] in the s and u compared to the t channel diagrams are still uncertain. In the QHD model, only a limited number of resonances (ones with lower spin) can be included whereas in the quark model a complete set of resonances are predicted. Indeed, for Compton scattering, Capstick and Keister found[12] that their model's sum over the s- and u-channel resonances could simulate the effect of t-channel exchanges (inherent in vector-dominance models) consistent with duality arguments. For now, t channel terms, such as the K^* shown in figure 3, are included in the QHD model, considered as a substitute for the missing s and u channel resonances[7]. A full listing of the NRQM resonances that need to be included in the s-channel can be found in reference [12]; their photocouplings have been calculated by many authors in various models (for a summary see reference [13]). The u-channel exchanges must include the ground-state and excited-state hyperons. Further resolution of the duality question must await more data and a detailed study of this reaction in the NRQM.

The predictions from the ABW calculation for the proposed measurements are shown by the solid curves in figure 4, at the kinematics of $W = 1.8$, $Q^2 = 1.0$, and $\epsilon = 0.7$. The four structure functions are plotted as a function of the momentum transfer to the kaon, $t = k^2 + k'^2 - 2k \cdot k'$ where k is the virtual photon 4-momentum and k' is the kaon 4-momentum. One interesting feature of these predictions is the strong dependence of the L/T ratio as a function of t, which could be easily checked by the proposed CLAS data at these and other neighboring kinematics. Another interesting feature is the prediction that the σ_{TT} term is very small. Measuring the TT interference term is of interest because it reveals the dependence of the amplitudes

upon the transverse polarization of the virtual photon. In real photoproduction experiments at 16 GeV photon energy[14], the σ_{TT} term was determined to be maximal, which was interpreted as the dominance of natural parity T-channel exchange. The interest here is to see how this term changes with Q^2 as the form factor of the kaon causes the dominant term to diminish, and also to study the variation of σ_{TT} with t.

In order to see the sensitivity of the ABW model to the N* resonances, we have repeated the calculations at the same kinematics but without the N*(1440) P$_{11}$ resonance. The results are plotted in the dashed lines in figure 4. The apparent reduction of σ_L, the different t-dependence for the σ_T, and the huge change in σ_{TT} are all indications of the sensitivity of this model to the removal of one N* resonance. These results are interesting, but one must remember that the parameters in the model are *fitted*, and so it is difficult to know if the calculations without the N*(1440) are real or are somehow an artifact of the fitting procedure.

1.2.2 The quark model

One strength of the NRQM is the relatively few parameters that it employs[15]. Many of the parameters are pre-determined from data on the nucleon resonances and their decays. The NRQM has also met with some success in describing Compton scattering at higher energies (about 1 GeV). Two groups have recently formulated quark models for kaon electroproduction. The publication by Ji and Cotanch[16] gives predictions for the kaon form factor from a quark model, although the calculation is fed into their hadrodynamic model. Also, Kumar and Onley[8] have calculated kaon photoproduction in a simplified NRQM. This has resulted in predictions which are in good agreement with the kaon photoproduction data with no additional free parameters. The Kumar/Onley calculation has been submitted for publication, and a detailed description is given in the attached appendix. This model is being extended for electroproduction, and predictions should be available in time for the oral presentation of this proposal.

1.2.3 Selectivity in the K^+ reaction channel

There are several advantages of studying the $^1H(e, e'K^+)$ reaction over that of the $^1H(e, e'\pi^+)$ reaction. The latter is dominated by the huge delta resonance, and there is no comparable dominant resonance in the strangeness-production channel. In addition, pion electroproduction has, at most kinematics, a substantial contribution from both the s and the u channels. The latter is an exchange term, which includes both the meson and the nucleon resonance in the propagator. For strangeness production, the u channel is suppressed due to the large mass of both the kaon and the hyperon in the propagator, so to first order the s channel contribution dominates, at least at forward kaon angles where the cross section is the largest. Under this approximation, the calculations appears much simpler, since the intermediate hyperon resonances (Y*) do not play a role in the s channel. Of course, this approximation must be tested when more sophisticated calculations are available.

Perhaps the most useful information comes when identification of the missing

mass determines the final state to be the Λ, an isospin-zero particle. By isospin conservation, the Δ resonances cannot contribute to the s channel. Hence the main contribution to the $^1\mathrm{H}(e, e'K^+)$ reaction is from the nucleon resonances in the s channel alone. (According to duality, only s and u channels should be included in a model where all nucleon resonances are used, to prevent double counting. Again, this assumption must be tested when more sophisticated calculations are available.)

The simplifying interpretation that the s channel dominates can be applied to the kaon photoproduction data as well. However, for the electroproduction data we can also examine the L/T ratio, which can change depending on the properties of the intermediate N* resonances[17]. At different values of the mass of the hadronic system W (i.e., on/off different resonances) we will search for any unusual values of L/T as compared to the calculations (at fixed Q^2), in particular for different recoiling hyperons. It has been suggested[15] that the orbitally excited N* resonances should decay most readily to hyperons with quark states of similar spin and orbital angular momentum. It will be particularly interesting to compare the $\Lambda(1405)$ and $\Lambda(1520)$ production ratios, which are respectively S_{01} and D_{03} resonances, compared to the P_{01} ground-state Λ [18].

There is an added bonus when the polarization of the Λ can be detected. We propose to detect the daughter proton from the Λ decay and to determine the asymmetry of the number of protons emitted up or down with respect to the K-Λ reaction plane. Large effects ($\sim 90\%$) in the Λ polarization have been observed in a kaon photoproduction experiment[19] at 5 GeV, as shown in figure 5, but the explanation is still not settled. We hope to provide data to test the two leading models of $s\bar{s}$ production, one being the $^3P_0$ model in which the $s\bar{s}$ pair has the quantum numbers of the vacuum, and the other being a gluonic pair creation model in which the pair has net angular momentum 1. The self-analyzing property of the Λ is another reason why $^1\mathrm{H}(e, e'K^+)$ is more selective than the $^1\mathrm{H}(e, e'\pi^+)$ reaction.

The contribution of the Δ^* resonances can be studied when the missing mass calculation determines the final state to the the Σ, an isospin-1 particle. A comparison of the L/T ratio for both Σ and Λ final states gives information on the role of the Δ^* intermediate resonances. The isospin dependence of kaon electroproduction shows interesting trends from the old data, as discussed below.

1.3 Previous data

The previous data for kaon photoproduction is scarce and of poor quality, as shown in the accepted CEBAF proposal[9] on this topic. The kaon electroproduction data is also scarce, with the extraction of the interference terms, σ_{TT} and σ_{TL} , having been performed only at low values of t [3] and having large errors, and the extracted values for the L/T [1] ratio also having large statistical errors, and again existing only at small values of t. The extracted L/T values for a Λ missing mass are shown in figure 6.

In parton models, when Q^2 is large compared to the quark masses, chirality conservation requires the L/T ratio to go to zero like $1/Q^2$ [20]. In fact, in this kinematic range the value of σ_L / σ_T for inclusive electroproduction is about 0.3 - 0.4. With

this in mind, the L/T ratio in figure 6 is perhaps larger than expected, but the large uncertainties prevent any real conclusion from being reached. In fact, QHD models in general predict that the L/T ratio for $K^+ \Lambda$ production should be large, but only for small values of t. It is also interesting that the same measurements[1] for a Σ^0 missing mass are consistent with zero, as shown in figure 6. This may be due to the effect of the intermediate Δ^* resonance contributions, as described above. We will search the kinematic range for any evidence of anomalously large values of σ_L / σ_T not predicted by either the QHD models or quark calculations. Such anomalies might signal new dynamics. [21]

An interesting feature in the L/T ratio is seen for the $^1H(e, e'\pi^+)$ data by the same group[22]. Here, the L/T ratio for a missing mass of the proton is quite large, whereas the L/T ratio for a missing mass of the Δ is very small, as shown in figure 7. This result is very intriguing in light of the (perhaps) small value of L/T in the $^1H(e, e'K^+)$ reaction to the Σ final state, where the intermediate Δ resonances may make a significant contribution.

There are other available data for the $^1H(e, e'\pi^+)$ reaction, with the Harvard data[23] being one of the most thorough in energy range near W=2.0 GeV. Here, the data are compared to a fixed-t dispersion model that improves on the model with Born terms (similar to the Born diagrams shown for QHD above) only. There are many ways to explore these data, as shown in reference [23], and their model calculations are in good agreement in most cases. A sample of their calculations of the interference terms is shown in figure 8, at kinematics where the longitudinal (scalar) contribution is large. Here, the σ_{TT} term is nearly as large as the transverse contribution, showing maximal polarization of the virtual photon perpendicular to the reaction plane.

A more recent calculation by Laget[11] for the σ_L and σ_T $^1H(e, e'\pi^+)$ cross sections is shown in figure 9. Here, at W=1.2 GeV, the longitudinal contribution is again dominant at $\theta_\pi = 0$, in the direction of the virtual photon. However, the integrated cross section shows the overall dominance of the transverse cross section, in the range $0.2 < Q^2 < 1.6$. Much can be learned by comparing the proposed measurements with the published $^1H(e, e'\pi^+)$ data in order to focus on the interesting features of the electroproduction reactions.

1.4 Summary: extracting the physics

The physics of kaon electroproduction may have some advantages in terms of theoretical simplicity when compared to pion electroproduction, due to the dominance of the nucleon resonances in the s channel only (to the Λ final state). The approved kaon photoproduction measurements will test these features at $Q^2 = 0$, but the $^1H(e, e'K^+)$ reaction can put tighter constraints on theoretical calculations, with data over a range of Q^2 and ϵ for all four structure functions.

It is particularly interesting to see how the L/T ratio changes with the isospin of the recoiling hyperon, and also to study this for different values of W corresponding to on/off the nucleon resonances. We will search for resonant behavior in W for all four structure functions. The large range in the kinematic phase space available to the CLAS detector will allow an untangling of such s-channel effects from other Q^2

8

dependences, such as that due to the kaon form factor.

Detection of the Λ polarization gives added information on the production mechanism of the $s\bar{s}$ pair. CLAS can, for some kinematics, measure the coincident Λ decay, which gives the Λ polarization, and may be sensitive to further details of the reaction mechanism.

Since this is unexplored territory, there is always the chance of discovering new N^* resonances or of seeing unexpectedly large values of L/T which could imply new dynamics beyond the conventional electroproduction models. But even without surprises, much can be learned from the ^{1}H($e, e'K^+$) reaction to explore whether the hadrodynamic or the more fundamental quark degrees of freedom are expressed in strange-particle production at CEBAF energies.

2 Experimental Overview

We present in this section our plan for studying the electroproduction of K^+ mesons from a hydrogen target. We propose to take data using the CLAS spectrometer in its "normal" magnetic configuration, that is, at maximum B field with the polarity chosen such that electrons are bent back towards the beam axis. We propose to detect the scattered electron, thus determining the four-momentum and polarization of the virtual photon; i.e. Q^2 , W and ϵ . We will also detect the produced K^+ , thus determining its azimuthal and polar angles (ϕ^* and $\cos(\theta^*)$) in the hadronic center of mass system. An alternative variable to $\cos(\theta^*)$ is t, the square of the momentum transfer from the virtual photon to the K^+ . The value of t is at a minimum when the K^+ is emitted along the direction of the virtual photon ($\cos(\theta^*) = 1$) and is at a maximum when $\cos(\theta^*) = $ -1.

We will collect data in the range of Q^2 from 1.0 to 2.5 GeV^2/c^2 , W from 1.6 to 2.3 GeV, at beam energies of 2.0, 2.4, 2.8, 3.2 and 4.0 GeV. We will perform a Rosenbluth separation over a portion of the Q^2 , W region covered, and will measure the ϕ dependence in the hadronic system to determine the four structure functions, σ_T , σ_L , σ_{TT} and σ_{TL} (see equation 1). We will perform the same structure function separation for different recoiling hyperons, specifically for the Λ , Σ , $\Lambda(1405)$/ $\Sigma(1385)$, and $\Lambda(1520)$. Structure function separations for kaon electroproduction have only been performed at small values of t, (see Ref. [1]) so we have designed the experiment to be able to do the structure function separation over the full range of t.

2.1 Experimental Plan

We have planned our data-taking to be compatible with other experiments doing electroproduction on hydrogen, so we will use a minimum bias trigger requiring an electron candidate track accompanied by at least one positively charged track. By measuring the 3-momenta of the electron and charged K^+ we will be able to bin each event uniquely according to the value of Q^2 , W, $\cos(\theta^*)$ and ϕ^* and mass of the recoiling hyperon, for each beam energy. We will know the acceptance and efficiency of the detector with respect to these six variables, integrating only over the over-all

azimuthal angle, Φ. The Φ dependence of any extracted quantity should be zero in the absence of beam or target polarization and so will provide a useful consistency check of the event analysis.

The four structure functions σ_T, σ_L, σ_{TT} and σ_{TL}, can be determined at a particular value of Q^2, W and t by comparing measurements at different values of beam energy and thus different values of ϵ. This "Rosenbluth" separation will be augmented by a fit to the ϕ^* dependence of the cross section, resulting in a complete separation of the four terms.

In the following sub-sections we will first show how the electron acceptance limits in terms of laboratory momentum and angle translates into the acceptance range in terms of Q^2 and ϵ. We then present a study of the CLAS acceptance and efficiency for detecting and identifying the K^+ as a function of its angles, $\cos(\theta^*)$ and ϕ^*, in the hadronic center of mass. Throughout this document, we illustrate details of the acceptance and background studies by considering the $Q^2 = 1.0$ GeV^2/c^2, W = 1.8 GeV point. The dominant background process is expected to come from the production of $\Delta^0\pi^+$ where the π^+ is mis-identified as a K^+. We estimate counting rates and justify our beam time request before discussing systematic errors and their effect on the Rosenbluth separation.

2.1.1 Electron Kinematics and Acceptance Limits

To detect an electron, it must traverse the drift chambers and Cerenkov counters and reach the electromagnetic shower counters. The region of momentum and scattering angle, θ_e for which and electron reaches the shower counters is shown in Figure 10. This figure is reproduced from the Conceptual Design Report, and was produced using the FAST Monte Carlo program[24]. It assumes that the toroidal magnet is run at full strength and with polarity corresponding to bending electrons inward toward the beam axis.

Figure 11 shows this acceptance limit transposed unto a Q^2 - ν plane for a particular beam energy, 4 GeV. The hatched area indicates the area available for electron scattering angles, θ_e, up to 90° and for W values above the $K\Lambda$ threshold. The smaller, cross-hatched region indicates the values of Q^2 and ν for which we can separate σ_L and σ_T using a Rosenbluth separation method.

To illustrate the experimental conditions in some detail, we show in Table 2 various characteristics of the electron and virtual photon for a data point of $Q^2 = 1.0$ GeV^2/c^2 and W = 1.8 GeV for beam energies ranging from 2.0 to 4.0 GeV, where p_e and θ_e are the electron momentum and angle, ϵ and θ_γ the virtual photon's polarization and laboratory angle, and p_k^{min} and p_k^{max} the minimum and maximum values of the kaon momentum in the laboratory for this value of Q^2 and W.

An important constraint for a Rosenbluth separation is that there be a significant span in ϵ for a given Q^2, W value. In order to easily see the range in ϵ covered by this experiment, we have plotted the various limits on the detection of an electron as a function of Q^2 and ϵ for three different values of W, (1.8, 2.0 and 2.2 GeV) which span the range of the experiment and show the result in Figure 12.

Figure 12 has four sub-plots. The figure in the upper left-hand corner shows the

Table 2: Event Kinematics for $Q^2 = 1.0$, W = 1.8

E_{beam}	2.0	2.4	2.8	3.2	4.0
p_e	0.21	0.61	1.01	1.41	2.21
θ_e	101.2	48.8	34.6	27.2	19.4
ϵ	0.07	0.37	0.55	0.67	0.80
θ_γ	5.75	12.9	16.2	18.3	20.9
p_k^{min}	0.136				
p_k^{max}	1.281				

accepted range of ϵ and Q^2 for detecting the electron for the case where W = 1.8 GeV. The various limits on the electron detection are identified. The upper limit on ϵ is set by the maximum beam energy of 4 GeV. The lower limit on Q^2 is set by the geometric limits on electron acceptance, to be explicit, for regions to the left of the accepted range the electron's momentum is too low (for it's angle) and it is swept into the forward "hole". The lower left-hand limiting line corresponds to an electron momentum of 200 MeV/c, below which special procedures, such as positron subtraction, must be enacted. Finally, the lower limit on ϵ is indicated by a line indicating an electron scattering angle of 90°.

We have used Figure 12 to indicate the data range of the experiment. The diamond symbols which lie along the upper curve or on the dashed lines indicate discrete Q^2 bins at a given beam energy. These data are collected simultaneously but are presented in discrete bins for the purpose of analysis. Five beam energies are indicated in the W = 1.8 GeV sub-plot, being 4.0, 3.2, 2.8, 2.4 and 2.0 GeV respectively as one goes lower in ϵ . The location of the data bins indicate that we will be able to do Rosenbluth separations for Q^2 between 1.0 and 2.5 GeV^2/c^2 for W = 1.8, for Q^2 between 1.0 and 2.0 GeV^2/c^2 for W = 2.0 GeV, and at a Q^2 of 1.5 GeV^2/c^2 for W = 2.2 GeV. Table 3 contains kinematic details for each of the 29 data points.

2.1.2 Kaon Kinematics and Acceptance Limits

The CLAS spectrometer has a large acceptance for the detection of outgoing positive particles, such as the K^+ . To see this, refer to Figure 13c in which the laboratory acceptance limits for kaon detection are plotted versus p_k and θ_k. This plot assumes that the K^+ must traverse all three regions of the drift chamber and strike the time of flight counters in order to be identified. Kaons with low momentum are "curled" up by the magnetic field and fail to reach the time of flight counters, while those with too small of a production angle go down the forward hole between the coils of the toroidal magnet.

Figure 13a shows the distribution in p_k and θ_k for kaons distributed isotropically in the center of mass for $Q^2 = 1.0$, W = 1.8 and $E_{beam} = 4$, while Figure 13b shows the same event distribution after running the FAST Monte Carlo [24] program and demanding event acceptance, that is, that the electron and kaon were both accepted

Table 3: Data Range: Expected Statistics and Acceptances

No.	E	Q^2	W	ϵ	p_e	θ_e	θ_γ	Acceptance	Counts / 100 Hrs.
1	4.0	1.0	1.8	0.80	2.21	19.4	20.9	0.23	21400
2	3.2	1.0	1.8	0.67	1.41	27.2	18.3	0.28	22500
3	2.8	1.0	1.8	0.55	1.01	34.6	16.2	0.27	19300
4	2.4	1.0	1.8	0.37	0.61	48.8	12.9	0.26	15800
5	2.0	1.0	1.8	0.07	0.21	101.2	5.8	0.04	1950
6	4.0	1.5	1.8	0.72	1.94	25.4	20.4	0.30	7200
7	3.2	1.5	1.8	0.53	1.14	37.4	16.8	0.30	6050
8	2.8	1.5	1.8	0.37	0.74	50.3	13.8	0.30	5200
9	2.4	1.5	1.8	0.14	0.34	84.9	8.2	0.04	650
10	4.0	2.0	1.8	0.63	1.68	31.7	18.9	0.31	2450
11	3.2	2.0	1.8	0.38	0.88	50.0	14.3	0.31	1950
12	2.8	2.0	1.8	0.18	0.48	75.5	9.8	0.05	270
13	4.0	2.5	1.8	0.52	1.41	38.9	17.0	0.33	950
14	3.2	2.5	1.8	0.22	0.61	68.9	10.8	0.05	120
15	4.0	1.0	2.0	0.71	1.80	21.5	15.9	0.02	1750
16	3.2	1.0	2.0	0.51	1.00	32.4	12.9	0.35	25500
17	2.8	1.0	2.0	0.33	0.60	45.2	10.2	0.35	22000
18	2.4	1.0	2.0	0.08	0.20	91.1	4.9	0.06	3000
19	4.0	1.5	2.0	0.60	1.54	28.6	15.5	0.37	9700
20	3.2	1.5	2.0	0.34	0.74	47.0	11.3	0.35	7300
21	2.8	1.5	2.0	0.13	0.34	78.0	6.9	0.06	1100
22	4.0	2.0	2.0	0.49	1.27	36.6	14.3	0.37	3500
23	3.2	2.0	2.0	0.18	0.47	70.3	8.3	0.07	500
24	4.0	2.5	2.0	0.37	1.01	46.4	12.4	0.37	750
25	3.2	1.0	2.2	0.28	1.36	24.8	11.6	0.04	22500
26	4.0	1.5	2.2	0.44	1.09	34.1	11.2	0.39	9500
27	3.2	1.5	2.2	0.10	0.29	78.9	5.2	0.06	1070
28	4.0	2.0	2.2	0.32	0.82	45.9	9.8	0.39	3700
29	4.0	2.5	2.2	0.18	0.56	63.9	7.6	0.06	250

and counted in the appropriate detector elements. The acceptance limits shown in Figure 13c are apparent in the depleted areas of scatterplot 4b.

We now discuss the kaon acceptance and efficiency in terms of the more relevant center of mass variables, $\cos(\theta^*)$ and ϕ^*. For the $Q^2 = 1.0$ GeV^2/c^2 , W = 1.8 GeV. point the 3-momentum of the virtual photon is 2.05 GeV/c. The K^+ can be emitted at any angle in the hadronic center of mass. If emitted backwards with a Λ recoiling, its laboratory momentum will be 0.136 GeV/c ; if forward, 1.28 GeV/c. Figure 14 shows the maximum and minimum kaon momenta for various values of Q^2 and W for the K^+ Λ final state. Note that the higher the value of Q^2 and/or W, the larger the spread between the minimum and maximum momentum values for the kaon. Dashed lines indicate momenta of 2.16 and 2.8 GeV/c which correspond to times of flight for pions as compared to kaons which differ by 3.3 σ and 2 σ, respectively. For the implications of this, see the Particle Identification section, below.

Figure 15a shows values of the K^+ laboratory angle plotted (in 5°contours) as a function of the hadronic angles $\cos(\theta^*)$ and ϕ^* for $Q^2 = 1.0$ GeV^2/c^2 , W = 1.8 GeV and $E_{beam} = 4.0$ GeV. Although details of this scatterplot will change for the various Q^2 , W, E_{beam} points, the basic features are always present. Backward angles in the center of mass (negative values of $\cos(\theta^*)$) correspond to large values of laboratory polar angle, θ_k. Note also that values of $\cos(\theta^*)$ near -1 correspond to low momentum, with values near 1 corresponding to high momentum. Also note the two areas of the plot with laboratory angles less than 10°. These are regions where the K^+ goes down the forward "hole", and is not detected.

2.1.3   Acceptance and Efficiency

We have modelled the acceptance of the detector using the parametric Monte Carlo program, FAST[24]. First, we generated the events using a simple program based upon the non-relativistic quark model which mimicked the observed Q^2 and W dependence of hyperon electroproduction data (see section on RATES for more details). We then studied the acceptance as a function of Q^2 , W, $\cos(\theta^*)$ and of ϕ^*. We separately studied the effect of electron geometrical acceptance and efficiency, of the K^+ geometrical acceptance, the K^+ decay probability, and the K^+ identification probability based upon a time of flight cut which excluded pions. We present summaries of these studies in Figures 15b, 15c and 16. Figure 15c shows the K^+ geometrical acceptance (once the electron is accepted) as a function of the center of mass angles; kaons with small laboratory angle (refer to Figure 15a) go down the 'hole' while low momentum kaons "curl up" before they reach the scintillator counters. In Figure 15b the lifetime efficiency is shown as a contour plot versus $\cos(\theta^*)$ and ϕ^*. Here it is obvious that those K^+ 's which are emitted at backward angles in the hadronic center of mass have lower momentum and thus a greater probability of decaying before reaching the time of flight counters.

In Figure 16 we show the over-all efficiency (for detecting both the electron and kaon) for the $Q^2 = 1.0$, W = 1.8, $E_{beam} = 2.4$ point as a function of $\cos(\theta^*)$ and of ϕ^* in the upper left and upper right sub-plots, respectively. The lower two plots shows the acceptance as a function of both angles, displayed in two different formats. The

areas of diminished acceptance at $\cos(\theta^*) \approx$ -1 corresponds to low-momentum kaons and the depletion is due primarily to kaon decay. Note also the depleted areas for $\cos(\theta^*) \approx 0.6$ with ϕ^* near 0 and 360°. These two areas correspond to K^+ 's going down the forward "hole".

2.1.4 Particle Identification and Backgrounds

Kaons can be positively identified by a measurement of their time of flight. The highest momentum kaons are going forward in the laboratory, where the flight path to the scintillator time-of-flight counter is about 5 meters. For small angles, the expected timing resolution of the scintillation counters is about 0.120 ns. Refer back to Figure 13c for an indication of the values of kaon momentum and angle for which the ideal pion time differs from the ideal kaon flight time by 0.400 ns, i.e. about 3.3σ. This means that if we make a timing cut of 1.65σ below the kaon ideal time, we will lose only about 10% of the kaons and will have a pion contamination of less than 10% of the pion/kaon ratio up to momenta of about 2.1 GeV/c.

We have studied the effect of these pions mimicking kaons by writing a special purpose 'background' event generator, and running these simulated events through the FAST Monte Carlo. The event generator produced pions in what we expect is a worst case scenario, that is, recoiling against a Δ_0 generated in exactly the same way as the K^+ and Λ for the signal. To normalize this background, we used the fact that the experiment of Bebek, et al. (see Ref. [25]) measured a K/π ratio of 0.1 to 0.2 in a similar kinematic range to ours.

To simulate this, we generated an event sample of 10 $\Delta_0\pi^+$ events for every Λk^+ produced, ran it through the FAST Monte Carlo, assuming that 1 in 10 pions was mis-identified as a kaon and display the results in Figure 17. Because of the 120 MeV width of the Δ_0, the π^+ background is distributed almost uniformly across the missing mass plot (Figure 17. Note that even in this case, the signal to noise ratio is greater than 10:1, and, since we should collect a large number of these background events in the same data sample, we will know the background shape well.

2.1.5 Counting Rates and Statistical Errors

The formula for the expected counting rate is given by

$$\frac{\text{RATE}}{\text{ACCEP}} = L \cdot \Gamma_T \cdot \sigma_V(Q^2, W) \cdot dQ^2 \cdot dW \tag{3}$$

and

$$\Gamma_T = \frac{\alpha}{4\pi} \frac{W}{ME^2} \frac{(W^2 - M^2)}{MQ^2} \frac{1}{1 - \epsilon} \tag{4}$$

where L is the luminosity, Γ_T the virtual photon flux factor, σ_V the total virtual photon cross section ($\sigma_T + \epsilon\sigma_L$) integrated over hadronic center of mass angles, and the other terms are bin sizes.

To calculate the counting rates for this experiment we have used the measured value of the unpolarized cross section as reported by Ref. [1] at $Q^2 = 1.2$, W=2.15.

We have ignored the interference terms σ_{TT} and σ_{TL} . We used a simple quark model calculation[26] to extrapolate from Q^2 =1.2 and W=2.15 to Q^2 =1.0, W=1.8. We also used calculations furnished to us by Bennhold to extrapolate the t-dependence of the cross section in order to estimate the unseen part of the total cross section.

The Harvard experiment[1] measured a cross section of about 275 nb/sr at Q^2 =1.0, W=2.15 GeV, ϵ =0.94. Simple assumptions about the W, Q^2 dependence[26] of the cross section allows us to estimate it to be 170 nb/sr at Q^2 =1.0, W=1.8. This cross section was measured for polar angle of the kaon in the center of mass, θ^*, up to 15°, or about 1.75% of the total solid angle. Using the t-dependence from the Bennhold calculations allows us to estimate that the 15° cut contained about 7.5% of the total number of events. This gives us our estimate of 500 nb for the angle integrated virtual photon cross section at Q^2 =1.0, W=1.8 GeV. We point out that this is lower than the estimate of about 1.4 μb from Bennhold, or a similar estimate from the toy quark model calculation. If we had assumed an isotropic angular distribution of the kaon we would have obtained 2.1 μb from the Harvard measurement.

However, we point out that the LAME experiment [4] did measure the total virtual photon cross section for similar kinematics to these ($Q^2 = 2.4$ GeV^2/c^2 and W = 1.9 GeV) to be only 68 ± 10 nbarns. Correcting for the Q^2 dependence gives us an estimate of 130 nbarns at $Q^2 = 1.0$, W = 1.8 GeV. The authors indicate that their systematic errors were on the order of 75 % for this measurement because of tracking inefficiencies associated with the secondary vertex of the decaying Λ. Because of the large systematic errors quoted, we have chosen to normalize our rate calculations to the average of the two estimates $(500 + 130)/2 = 315$ nb, at Q^2 =1.0 GeV^2/c^2 , W=1.8 GeV and $\epsilon = 1$, and use the simple quark model to calculate the cross section at other values of Q^2 , W and ϵ . Note that, since we are dominated by systematic errors (see section below), that the experimental errors do not increase significantly even if the lower rate estimate from the LAME experiment is valid.

We have based our beam time request on the condition that the statistical errors be smaller than the estimated systematic error of 7% over most of the kinematic range of the experiment. Following this prescription we conclude that we will require 100 hours of beam time for each energy. In addition to kinematic details, Table 3 contains our calculations for the overall event acceptance and expected total counts for each of the 29 data points indicated in Figure 12.

2.2 Structure Function Separation

2.2.1 Rosenbluth Separation

From the form of the equation for the virtual photoproduction cross section it follows that in order to separately determine the values of the four individual structure functions, σ_T , σ_L , σ_{TT} and σ_{TL} it is necessary to perform a Rosenbluth separation. The procedure is to measure the cross section at several values of E_{beam} , for fixed values of Q^2 and W. The ratio σ_L / σ_T has phenomenological interest because it is sensitive to the spin of the object which absorbs the virtual photon. A large value is associated

Table 4: A list of various sources of systematic errors including a description of the error, a size estimate, and an estimate of its effect on the cross section. Correlated errors are added linearly, uncorrelated subsets are added in quadrature.

Source of Error	Description of Error; Size of Effect	Size of Error in Cross Section	Sum
Acceptances	Geometrical Acceptance and Efficiencies; 20% to 40%	3%	3%
Angular Determination (absolute)	Offset of Angle 1 mrad	2.5% (small angle) 1% (large angle)	5%
Momentum Determination (absolute)	Offset of Momentum 0.5%	1.5%	
Beam Energy Determination (absolute)	Offset of Energy 0.3 %	0.9 %	
Electron Efficiency, Pion Misidentification	2%	2%	2%
Kaon Efficiency, Pion Misidentification	2%	2%	2%
Radiative Corrections	16% corr. (20 deg.) 38% corr. (50 deg.)	2%	2%
Total	7%		

with absorption on a spin 0 object (for example, a meson) and a small value with absorption by a spin 1/2 object such as a quark. However, the L/T ratio is difficult to measure since few systematic errors cancel at the different values of E_{beam}.

The accuracy on the measurement of the ratio is proportional to the separation in ϵ between the different energy measurements at a common Q^2 and W point. The formula for the error on the ratio R $= \sigma_L / \sigma_T$ is straightforward to calculate but somewhat cumbersome to derive. In the case where the errors on the individual virtual photoabsorption cross sections are equal, the error on R is given by

$$\delta R^2 = \frac{(\frac{\delta\sigma}{\sigma})^2}{\Delta\epsilon^2} \cdot 2 \cdot (1 + \bar{\epsilon}R + \bar{\epsilon^2}R^2) \tag{5}$$

where $\delta\sigma/\sigma$ is the fractional error on the cross section, which is dominated by the systematic error.

Table 4 summarizes the sources and sizes of individual systematic errors leading to this estimate. Summing the correlated errors linearly and the uncorrelated subsets in quadrature leads us to estimate 7% as a likely maximum systematic error on individual cross section measurements. We feel that this accuracy can be achieved in the first year of analysis. It is probable that several years' experience with the CLAS spectrometer will lower this error.

Figure 18 shows an example of what the data at a Q^2 of 1.0, and W of 1.8 might

look like. Here we have plotted the differential cross sections divided by the photon flux factor, Γ_T, versus ϵ . The error bars shown are the 7% systematic errors. The extracted values and errors on σ_L and σ_T are also shown.

Figure 19 displays what we might expect for errors if we plot the ratio (σ_L /σ_T) versus t at $Q^2 = 1.0$ GeV^2/c^2 and W = 1.8 GeV. The data point at t_{min} with the large error bars is from the experiment of Bebek, et al. [1]. The smaller (included) error bars are what we expect from our error analysis; in addition, we will simultaneously measure the other four points at higher values of t. The curve is from a calculation by Cotanch and Williams [27] and gives an idea of the size of the effects which might be observed for this reaction.

The Rosenbluth separation determines the structure functions σ_L and σ_T separately and not just the ratio. The main objective of our proposal is to obtain precision measurements for all four structure functions. In order to illustrate the expected errors for σ_L as a function of $\cos(\theta^*)$, figure 20 plots the statistical plus systematic errors for the proposed measurements at Q^2 =1.0, W=1.8 and $\epsilon = 0.7$ on top of a calculation by Bennhold [28].

2.2.2 Extraction of the Interference Terms

An expanded form of Equation 1 has been given by Cotanch: [7]

$$\frac{d\sigma_v}{d\Omega_k} = \frac{d\sigma_U}{d\Omega_k} + \epsilon\frac{d\sigma_P}{d\Omega_k}\sin^2\theta\cos2\phi + \epsilon_L\frac{d\sigma_L}{d\Omega_k} + (2\epsilon_L(\epsilon+1))^{1/2}\frac{d\sigma_I}{d\Omega_k}\sin\theta\cos\phi \qquad (6)$$

This form explicitly shows the θ dependence of the individual terms. The $\sin(\theta)$ or $\sin^2(\theta)$ dependence of the interference terms makes them difficult to measure by experiments which concentrate on the low-t region. As we have shown, this experiment has large acceptance for K^+ produced at large values of t, thus we should be sensitive to ϕ dependence in the cross section at a low level. This sensitivity is estimated to be on the order of 3% (see Table 4), depending on the bin size in ϕ. We note that large values of σ_{TT} have been measured in a real photoproduction experiment using a polarized bremsstrahlung beam [14], which the authors interpreted as the dominance of natural parity t-channel exchange processes. It will be interesting to observe the size of both σ_{TT} and σ_{TL} for the proposed measurements.

2.3 Λ Polarization Measurement

In addition to detecting the K^+ , we are able to measure the polarization of the Λ relative to the normal to the hadron reaction plane by detecting the proton only. We will measure the number of protons going "up" (U) relative to the hadron plane, and the number going "down" (D). The polarization of the Λ is simply related to the asymmetry between these two numbers:

$$P = \frac{2}{\alpha}\frac{(U - D)}{(U + D)} \qquad (7)$$

where α is the analyzing power of the parity violating weak decay of the Λ, $\alpha = 0.642$. For example, if the Λ is 100% polarized, 2/3 of the protons will go "up" and 1/3 "down".

For most of the kinematic range of this experiment, the proton acceptance is sufficiently large ($> 50\%$) to give the polarization to a few percent. We expect that the systematic errors on this measurement will also be quite small unless there is a strong correlation between the value of the polarization and regions of the kinematic space where the interference terms (σ_{TT} and σ_{TL}) are large. If σ_{TT} is maximal, for instance, the hadron plane will be crossed with the electron plane and "up" will correspond to large laboratory angles, while "down" will correspond to small angles, and thus lower acceptance. We have not yet done a detailed analysis of this possible correlation.

2.4 Controls and Calibration

The systematics of the data analysis can be further reduced by judicious use of various controls, in general, ratios of structure function values for different kinematic conditions. The idea is that some of the sources of systematic error cancel in the ratio. Examples of these ratios include measuring σ_L , σ_T etc. for the following cases: a) for $\cos(\theta^*)$ negative versus positive, b) for Λ recoil versus Σ recoil, and c) for different values of W, for example at the $N^*(1710)$ resonance and at higher W.

This experiment relies on careful calibration of the instrumentation. Accordingly, we will need additional beam time for the express purpose of calibrating the tracking systems of the CLAS. As shown in Table 4, the dominant systematic errors have to do with uncertainty in the absolute values of scattered momentum and angle. We thus request beam time in which the CLAS will run with a "point" CH_2 target, with an angle-defining "sieve slit" affixed downstream of the target. This setup will allow us to define fixed angles relative to the beam direction. By observing the position of the elastic peak at these fixed angles, we will have tracks of known momentum and angle against which to calibrate the tracking system. A simple estimate of running time assumes that we collect data at 5 values of θ, 3 target positions, and 3 values of B field. If we collect 10,000 counts at each of these points and for each of the 6 sectors of the CLAS, we will need $2.7 \cdot 10^6$ events. At a counting rate of 100 events/s, this requires about 8 hours at each beam energy.

3 Summary

We conclude the experimental section with the following remarks:

1. The CLAS detector has large acceptance for electron and kaon detection (20-40%), for the data range proposed here.

2. Large and uniform acceptance in $\cos(\theta^*)$ and ϕ^* allows a reliable determination of the t- and ϕ-dependence of the cross section, and thus separation of the four structure functions.

3. We can achieve measurements with small statistical errors (typically less than 3%) in 100 hours of beam time.

4. Systematic errors of about 7% will dominate the errors on the four structure functions. Propagation of errors will result in errors of $> 20\%$ or more for the ratio σ_L / σ_T .

5. Careful attention to calibrations is necessary. We anticipate requiring one to a few days' beam time for this express purpose.

6. We request 100 hours of beam time at energies of 2.0, 2.4, 2.8, 3.2 and 4.0 GeV. The first and last energies are compatible with previously approved N* experiments, and thus we are requesting 300 hours of new beam time.

References

[1] C.J. Bebek, et al., Phys. Rev. D15, 3082 (1977).

[2] P. Brauel, et al., Z. Phys.C3, 101 (1979).

[3] T. Azemoon, et al., Nucl. Phys.B95, 77 (1975).

[4] C.T. Day, et al., Phys. Rev. D23, 576 (1981).

[5] F.J. Barbosa, et al., NIM A323, 191 (1992).

[6] R. Adelseck, Ph.D. thesis, Ohio University, 1988; R.A. Adelseck and L.E. Wright, Phys. Rev. C38, 1965 (1988); C. Bennhold and L.E. Wright, Phys. Rev. C39, 927 (1989); R.A. Adelseck and B. Saghai, Phys. Rev. C42, 108 (1990).

[7] R.A. Williams, C-R. Ji, and S.R. Cotanch, Phys. Rev. C46, 1617 (1992)

[8] A. Kumar and D.S. Onley, submitted to Phys. Rev. C.

[9] R. Schumacher, CEBAF proposal E-89-004.

[10] T.W. Donnelly and A.S. Raskin, Ann. Phys. 169, 247 (1986).

[11] J.M. Laget, Can. J. Phys. 62, 1046 (1984), and references therein.

[12] S. Capstick and B.D. Keister, Phys. Rev. D46, 84 (1992); Phys. Rev. D47, 860 (1993).

[13] S. Capstick, Phys. Rev. D46, 2864 (1992).

[14] D.J. Quinn, et al.,Phys. Rev. Lett.34, 543 (1975).

[15] N. Isgur, IJMP E1, 465 (1992), and references therein.

[16] C.-R. Ji and S.R. Cotanch, Phys. Rev. D41, 2319 (1990).

[17] S. Capstick, private communication.

[18] Particle Data Group, Phys. Rev. D45 Part 2 (1992).

[19] G. Vogel et al., Phys. Lett. 40B, 513 (1972).

[20] R. Jaffe, Phys. Rev. D11, 1953 (1975). C.G. Callan and D.J. Gross, Phys. Rev. Lett. 22, 156 (1969).

[21] Large values of L/T could be attributed to the virtual photon being absorbed by a spin-zero diquark. See, for instance, S. Ekelin and S. Fredriksson, Phys. Lett. 162B, 373 (1985).

[22] C.J. Bebek, et al., Phy. Rev. Lett. 38, 1051 (1977); C.J. Bebek, et al., Phys. Rev. Lett. 37, 1326 (1976).

[23] C.N. Brown, et al., Phys. Rev. D8, 92 (1975).

[24] E. S. Smith, FAST Monte Carlo Program, CLAS Note 90-003.

[25] C.J. Bebek, et al., Phy. Rev. Lett. 32, 21 (1974).

[26] The unpolarized transverse virtual photoabsorption cross section, σ_T , can be expressed in terms of quark distribution functions and kinematic factors, as follows:

$$\frac{4\pi^2\alpha}{M^2}\frac{M^2}{W^2-M^2}(\frac{4}{9}u_v(x))f_k, \tag{8}$$

where $u_v(x)$ is the up-quark momentum distribution in the proton which we have taken from the thesis of Bodek to be approximately $4(1-x)^4$, and f_k is the probability that the final hadronic state will be a Λ K^+ state, which we take as 0.05. This form for σ_T is in good agreement with the dependence seen in reference [1].

[27] Plot furnished by Robert A. Williams and Stephen R. Cotanch; private communication.

[28] Cross section furnished by Cornelius Bennhold; private communication.
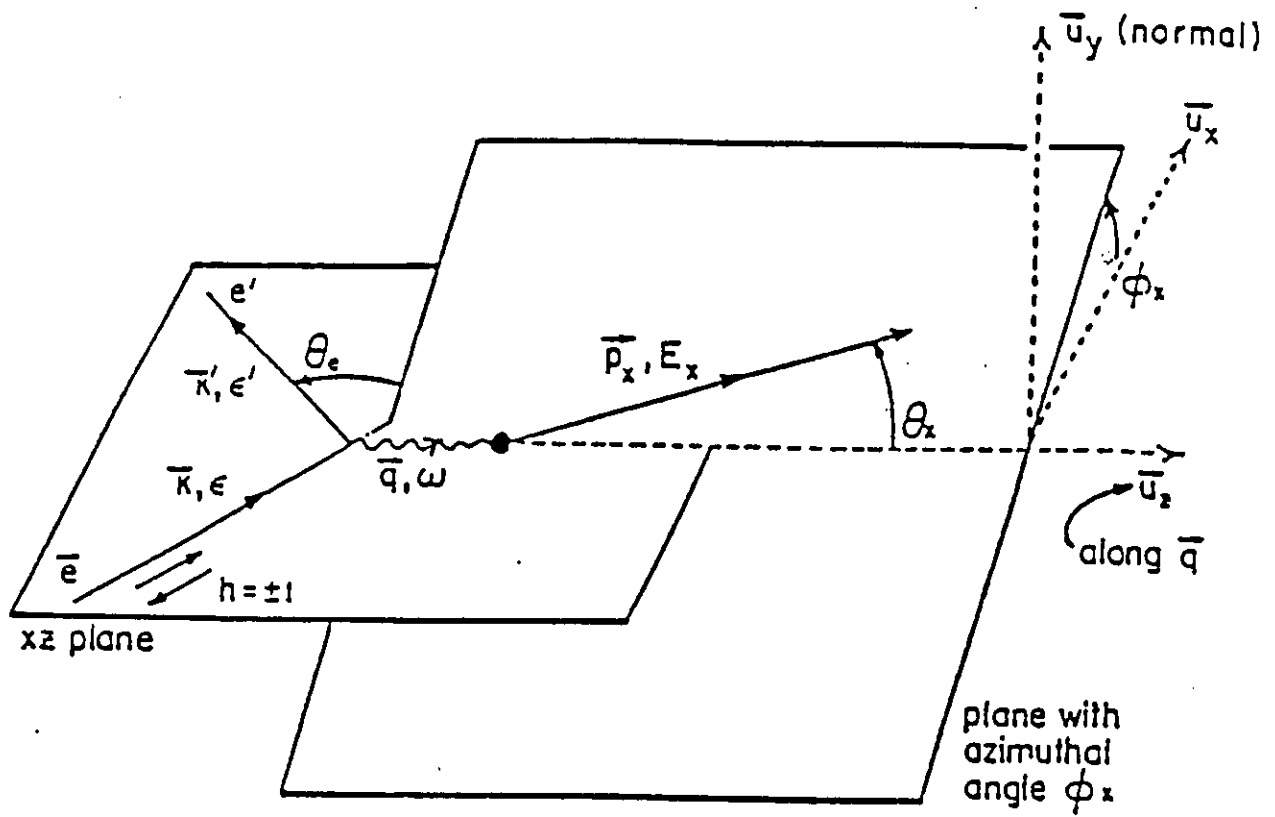
Figure 1: The reaction plane for $(e, e'X)$.
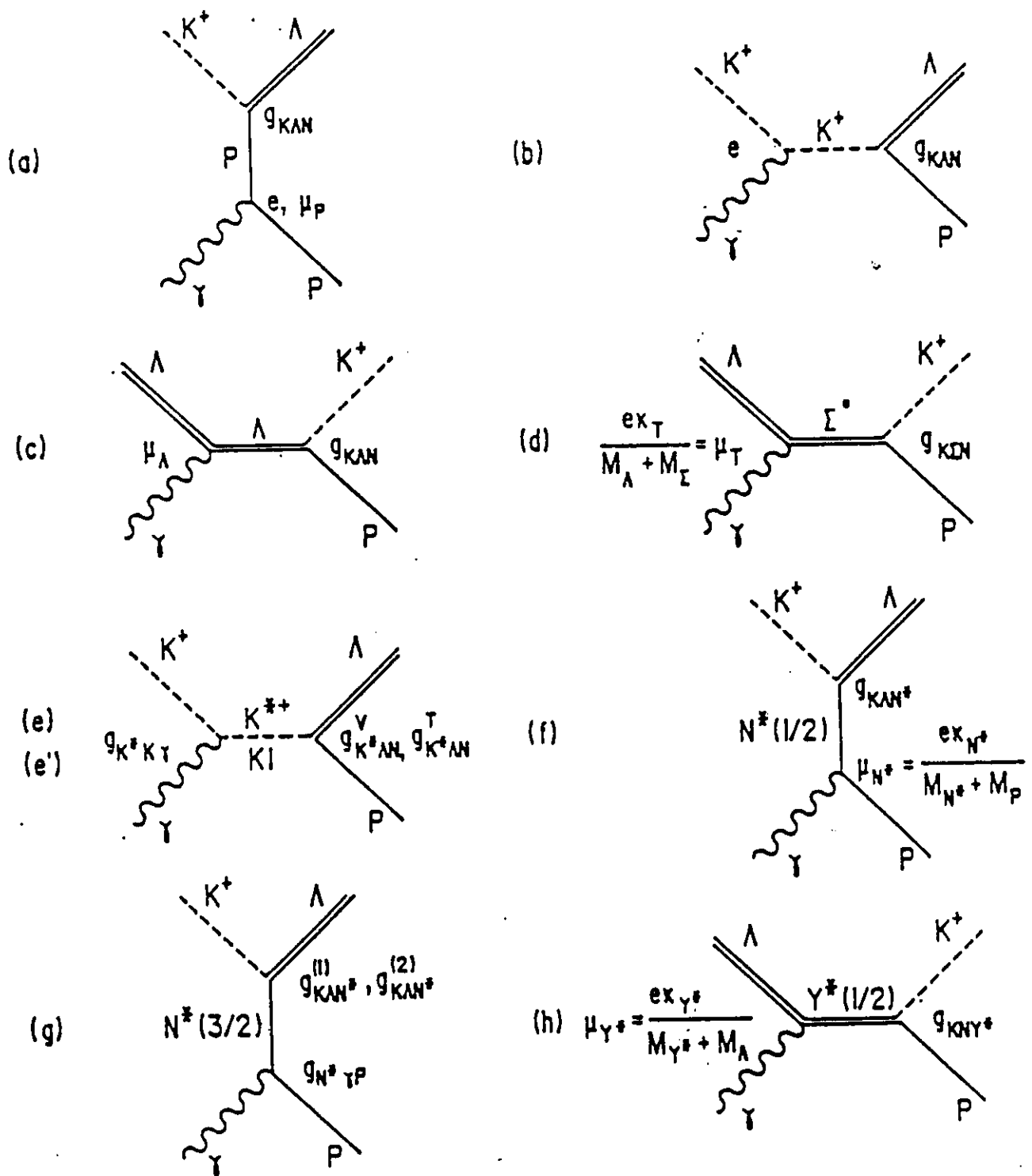
Figure 2: The diagrams used in the nucleon/meson-exchange model.

$p(\gamma, K^+)\Lambda$

$d\sigma/d\Omega$

$(\mu b/sr)$

$\theta_{c.m.} \sim 27^\circ$

E_γ (Gev)

$p(\gamma, K^+)\Sigma^\circ$

$d\sigma/d\Omega$

$(\mu b/sr)$

$\theta_{c.m.} \sim 28^\circ$

E_γ (Gev)
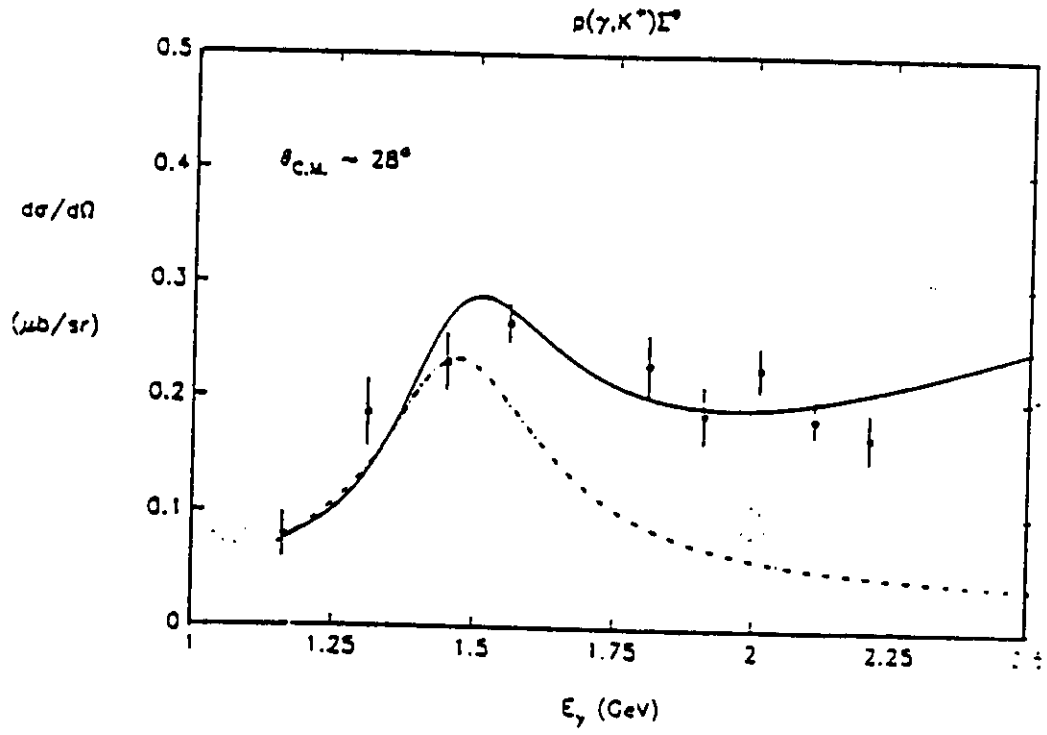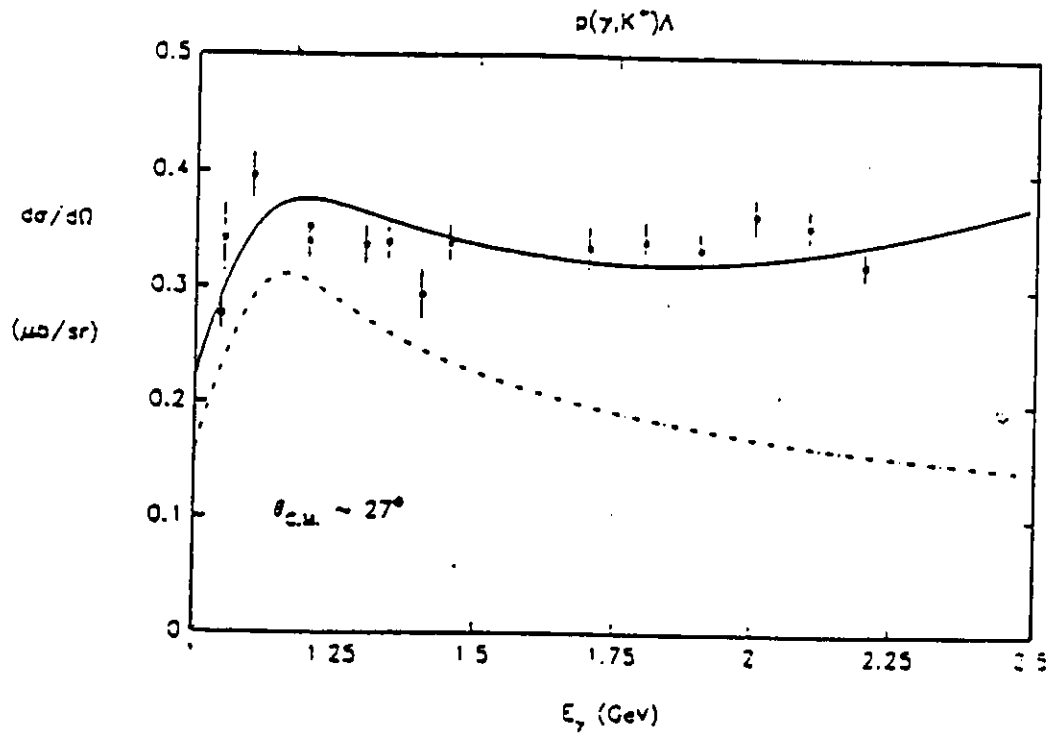
Figure 3: The effect of including the $K*$ resonance in the t channel.
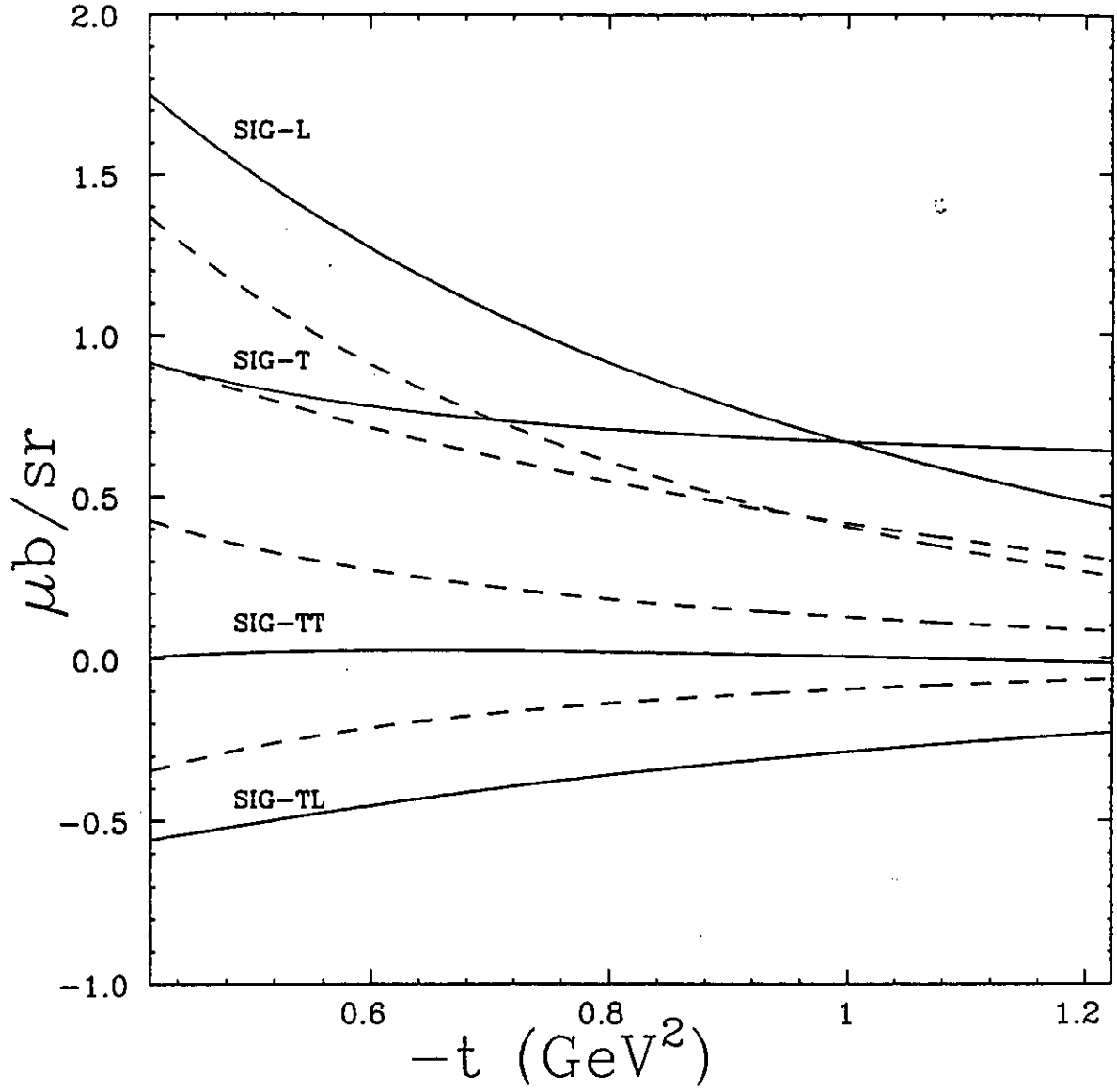
Figure 4: Calculations in the ABW model at kinematics of $W = 1.8$ GeV, $Q^2 = 1.0$ GeV^2, and $\epsilon = 0.7$. The dashed lines has removed the N*(1440) intermediate resonance.
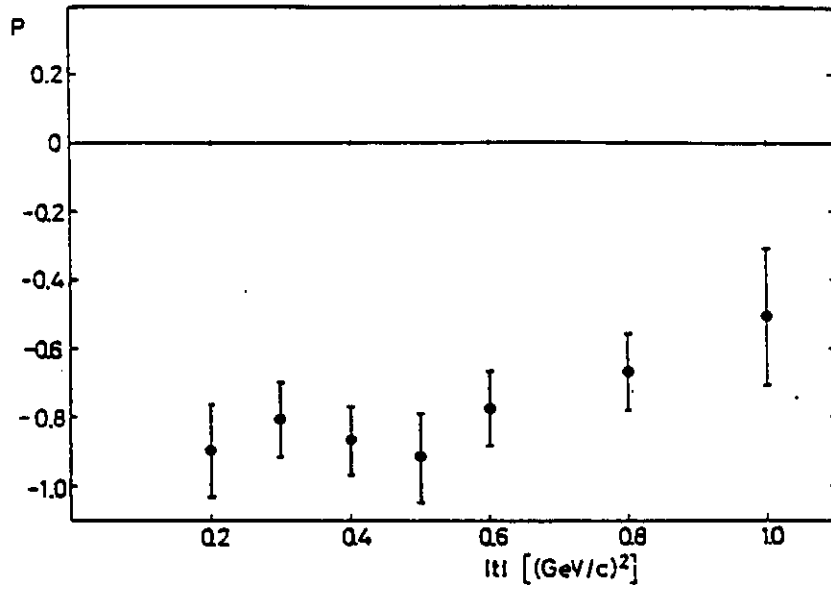
Figure 5: The Λ polarization in $\gamma p \rightarrow K^+ \Lambda$ at 5 GeV (using the Basel sign convention).
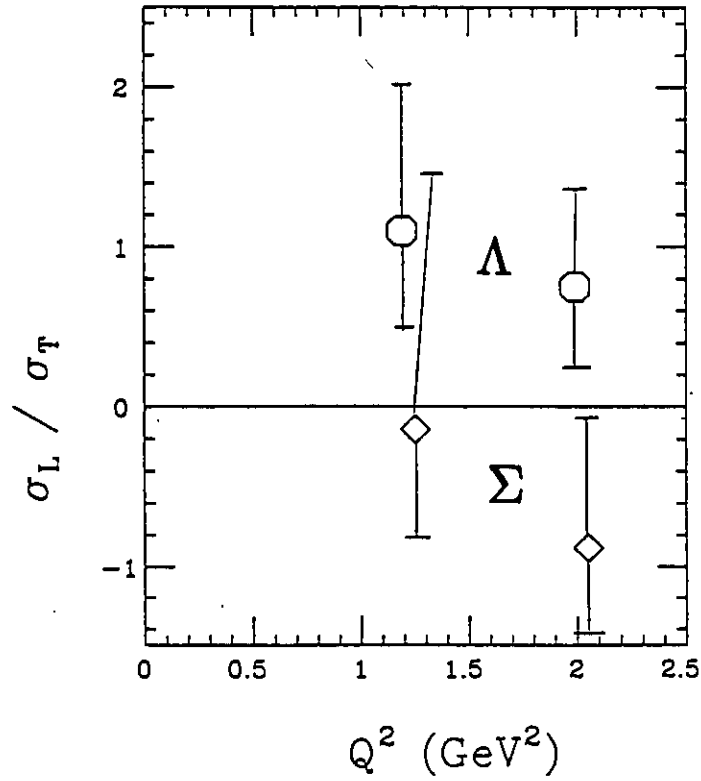
Figure 6: Data for the $^1\mathrm{H}(e, e'K^+)$ reaction to the Λ and Σ^0 final states.
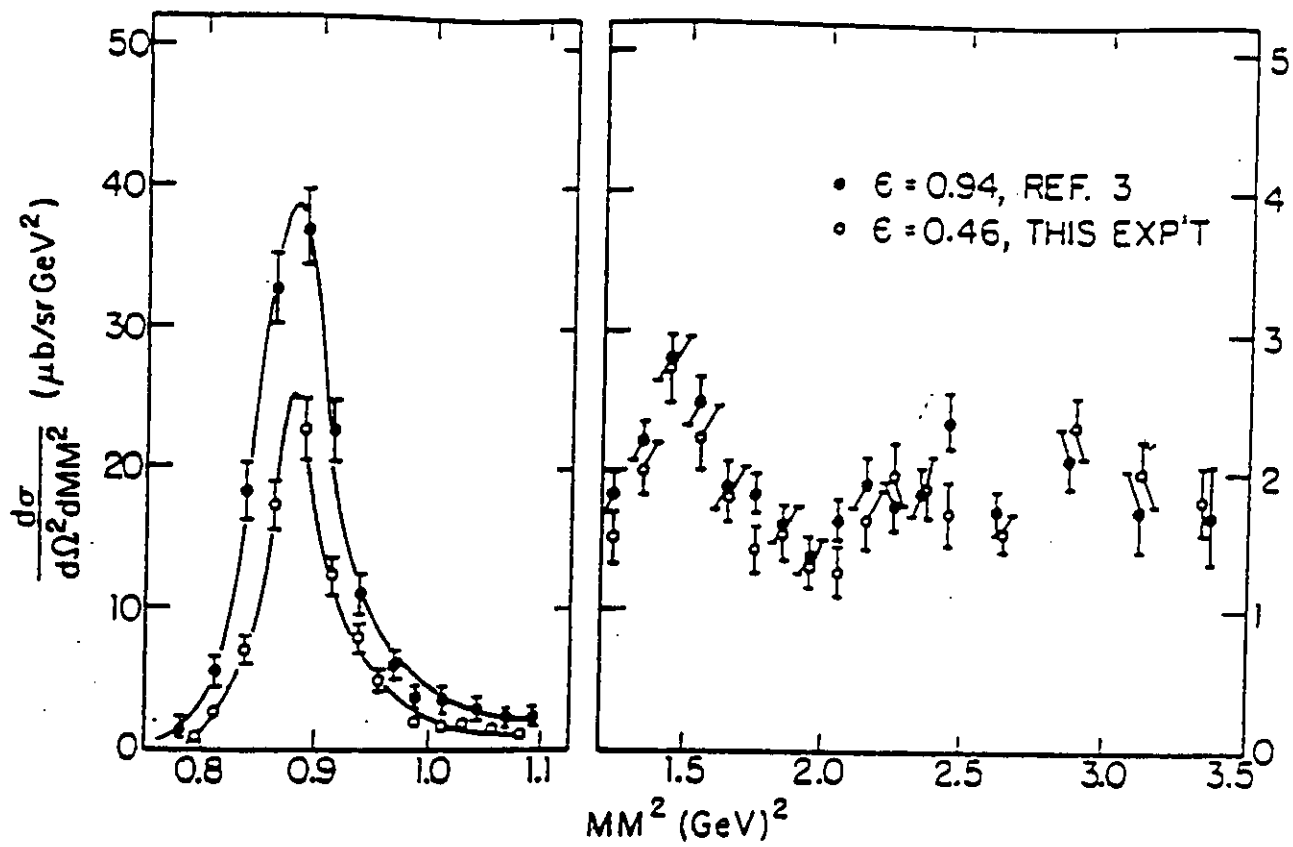
Figure 7: Data for the $^1H(e, e'\pi^+)$ reaction as a function of missing mass.
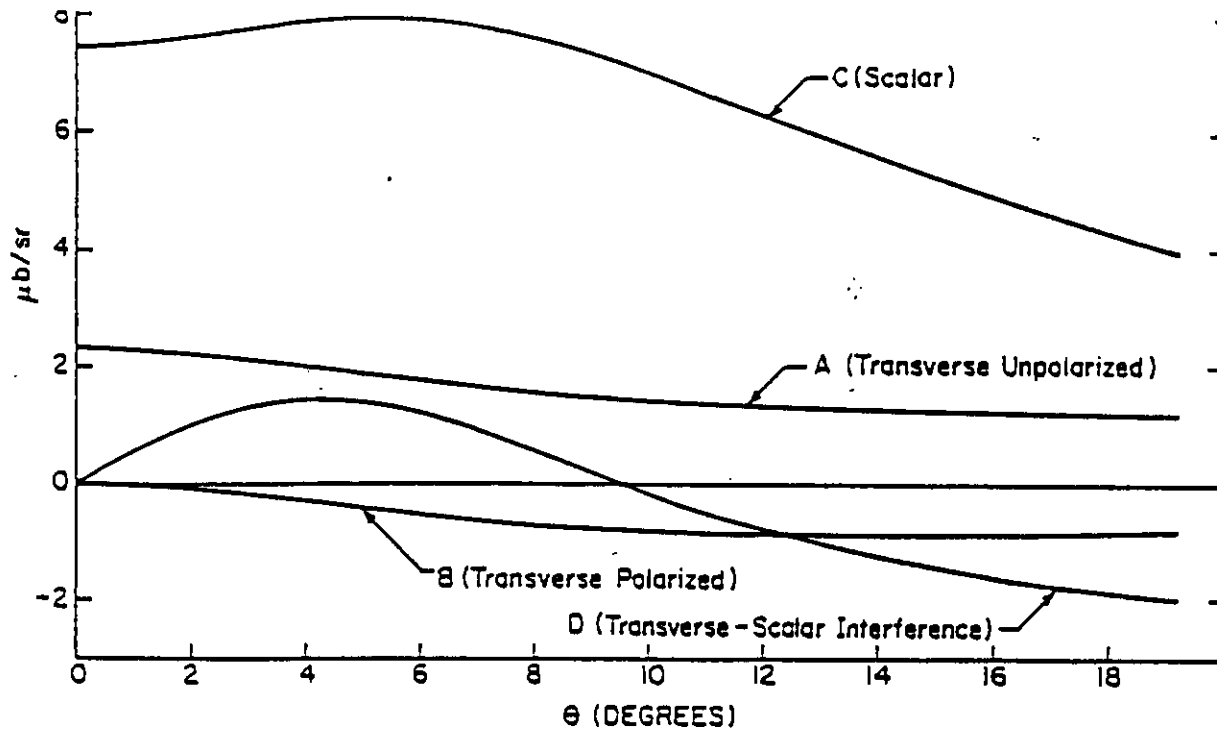
Figure 8: Calculations for the $^1H(e, e'\pi^+)$ reaction in the fixed-t dispersion model.
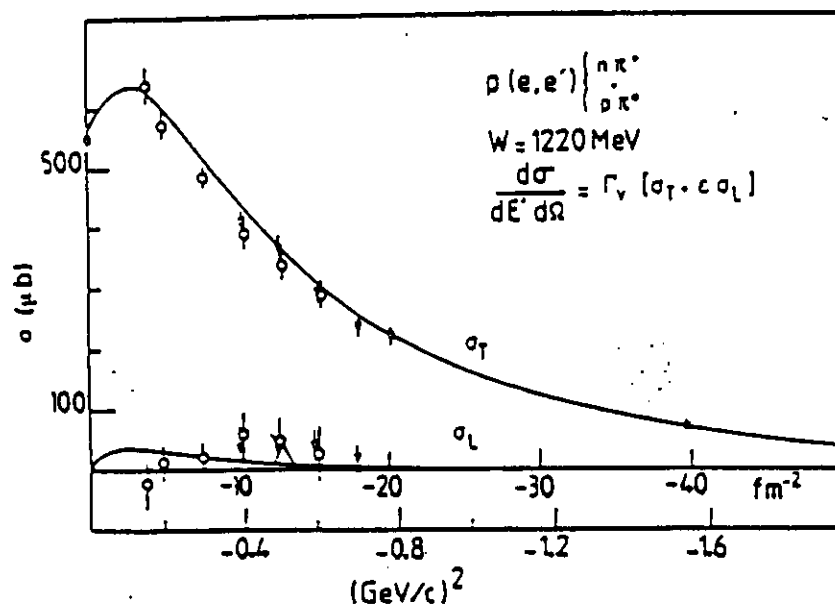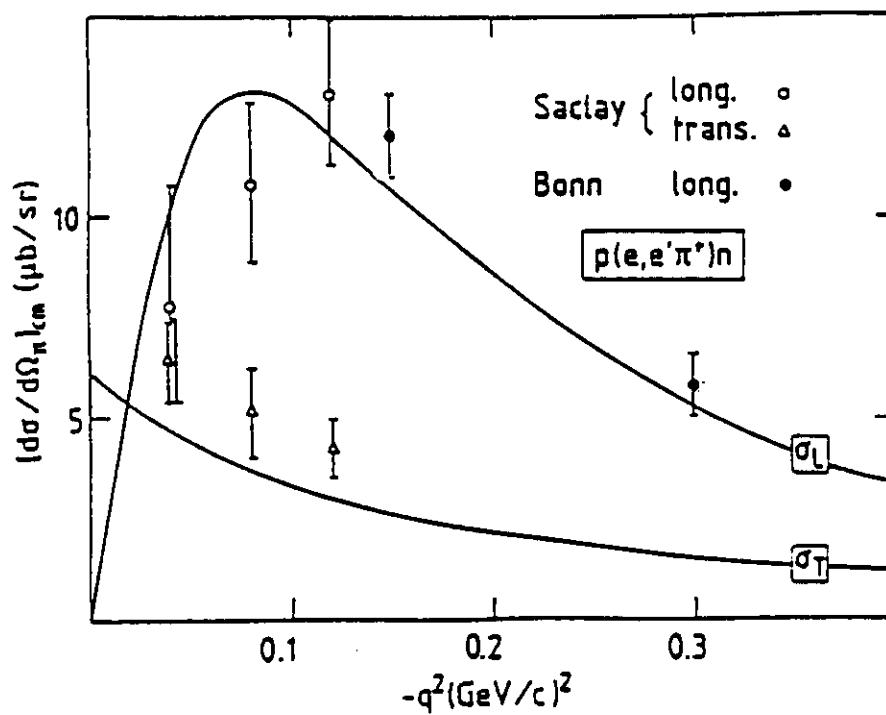
Figure 9: Calculations compared to longitudinal and transverse cross sections for the $^1H(e, e'\pi^+)$ reaction by Laget.

CLAS Acceptance – INBENDERS
Shower Counter (90° Sector)
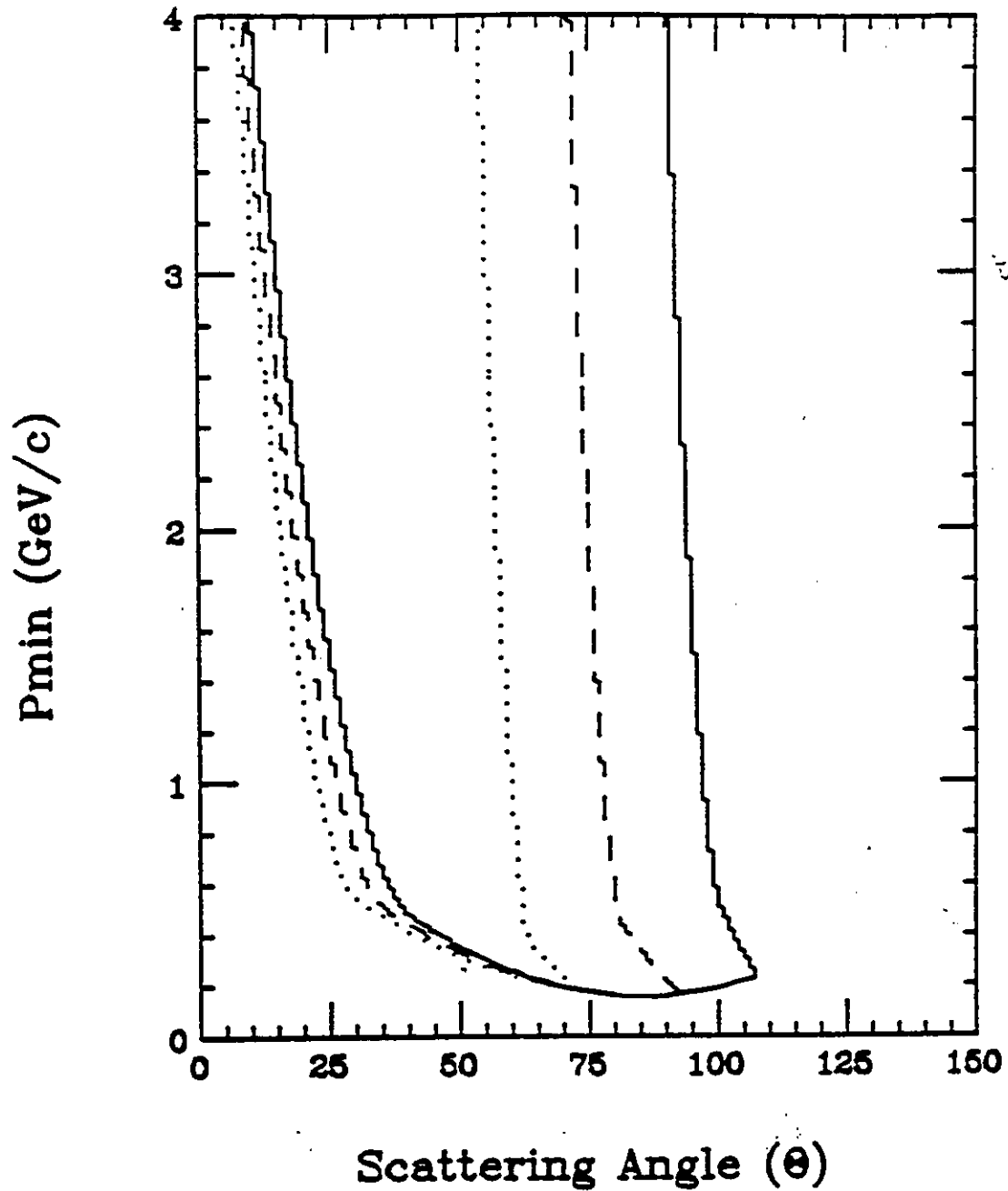
Figure 10: Electron Acceptance Limits: p_e vs. θ_e

ep Kinematics (E_beam=4GeV)
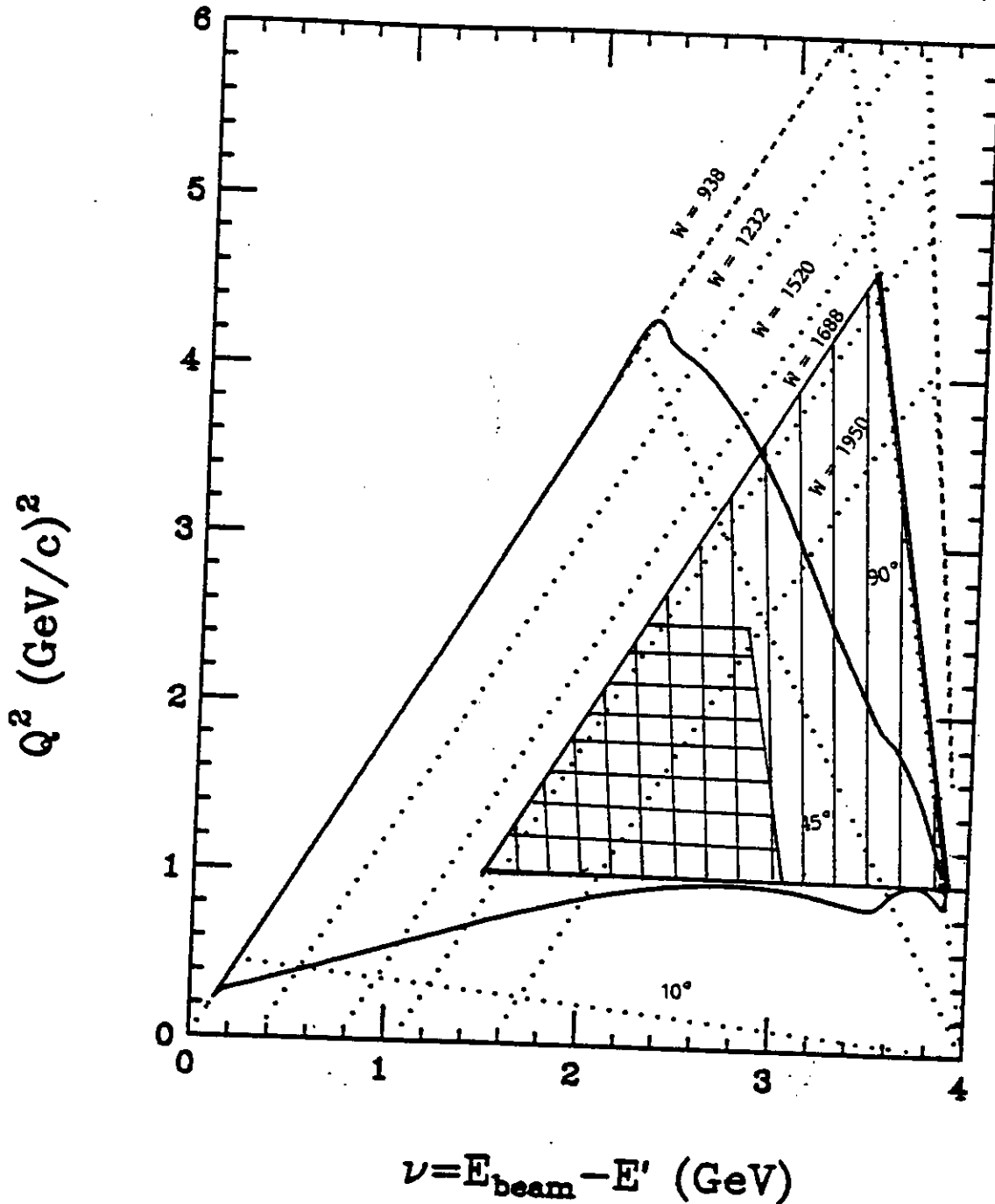
Figure 11: Electron Acceptance Limits: Q^2 vs. ν , for E_{beam}=4.0 GeV. Hatched region covered by this experiment, cross-hatched area is the region where we can perform a Rosenbluth separation.
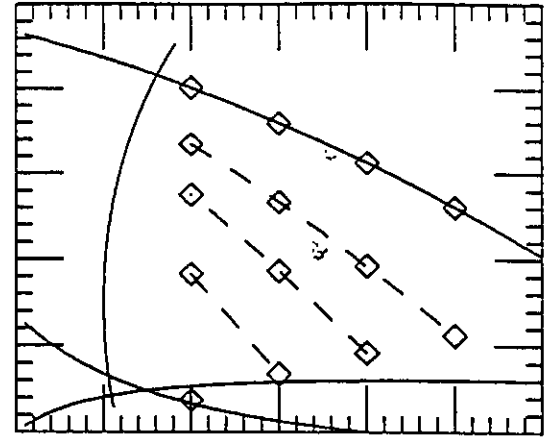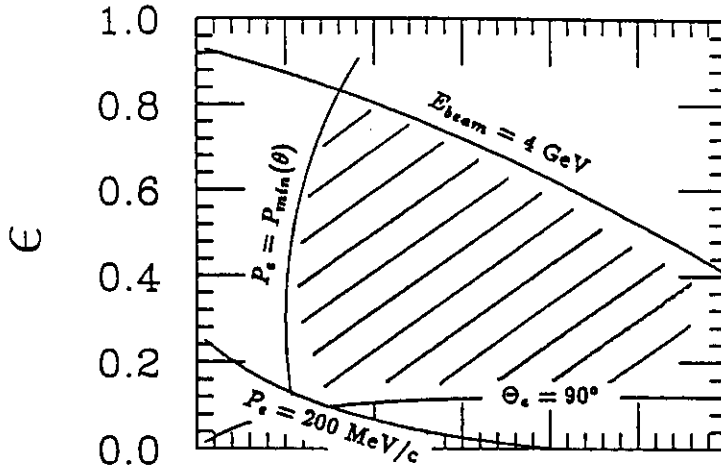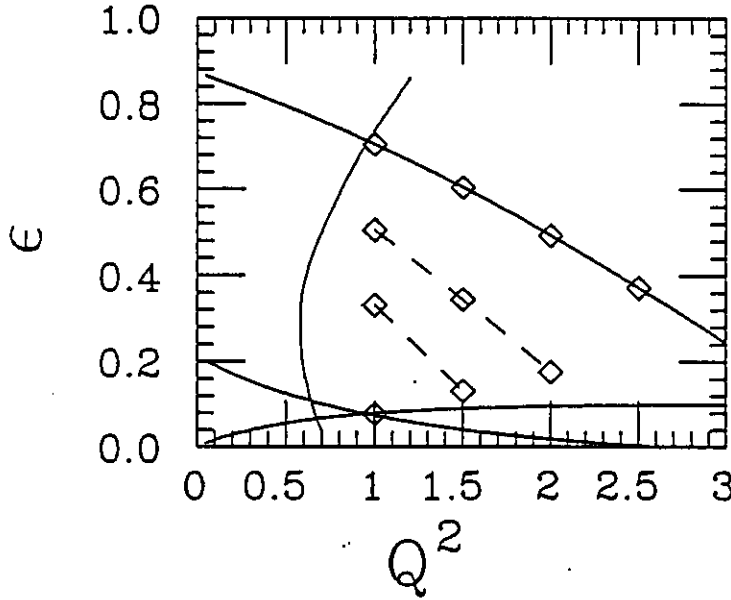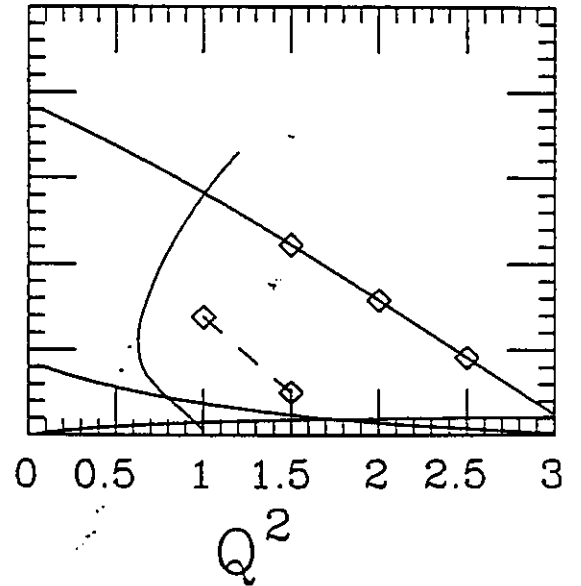
Figure 12: The upper left-hand plot shows the region of non-zero acceptance for the scattered electron as a function of Q^2 and ϵ. The sources of limitation are indicated. The other three sub-plots show the location of the 29 data bins constituting the data sample for this experiment. Dashed lines connect data bins for the same beam energy. Table 3 contains detailed information about each of these data points.
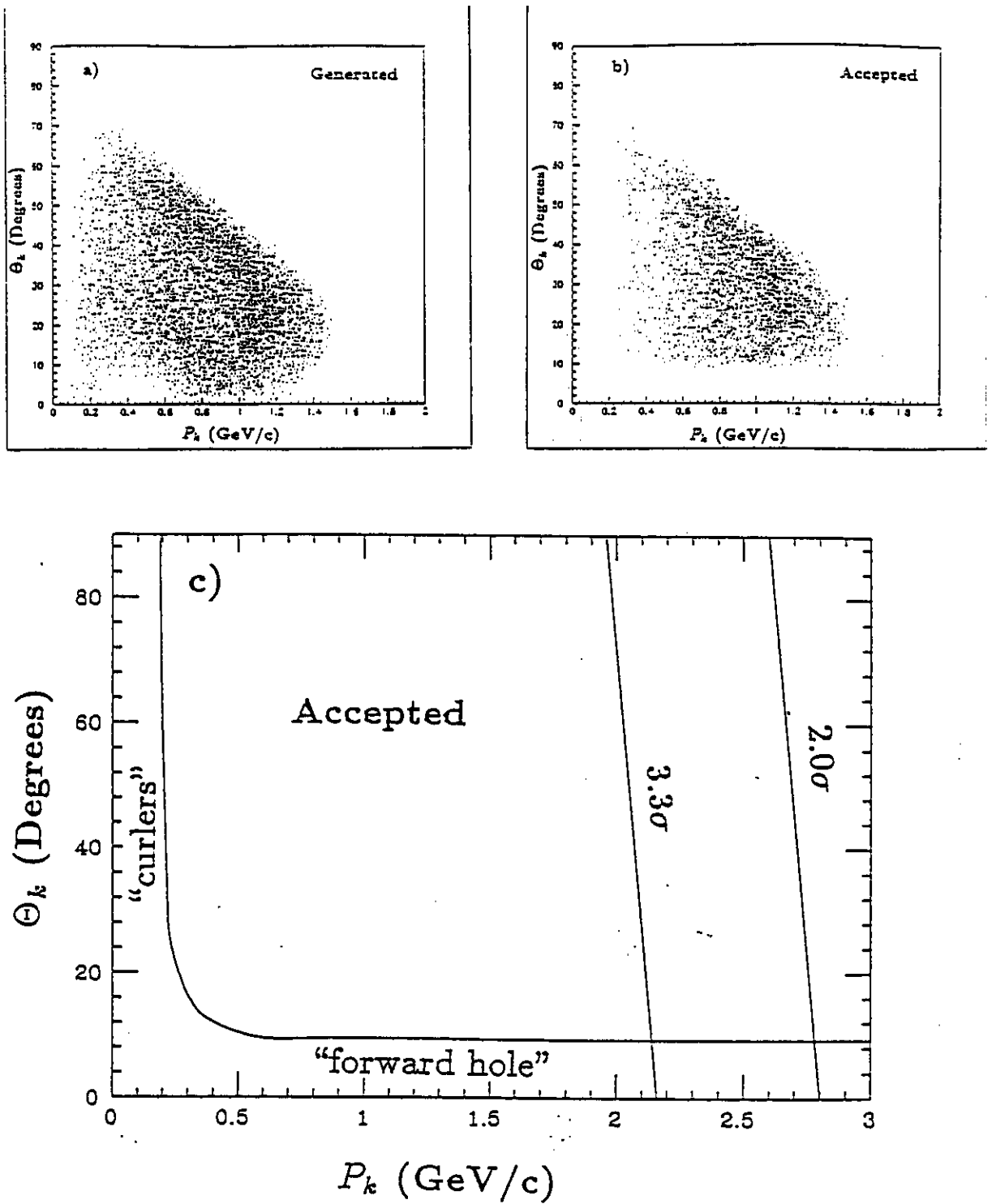
Figure 13: Kaon Acceptance Limits: p_k vs. θ_k. a) shows a scatterplot of kaons generated isotropically in the hadronic c.m. ($Q^2 =1.0$, W=1.8, E_{beam}=4.0), b) shows the accepted distribution, and c) shows the acceptance limits.
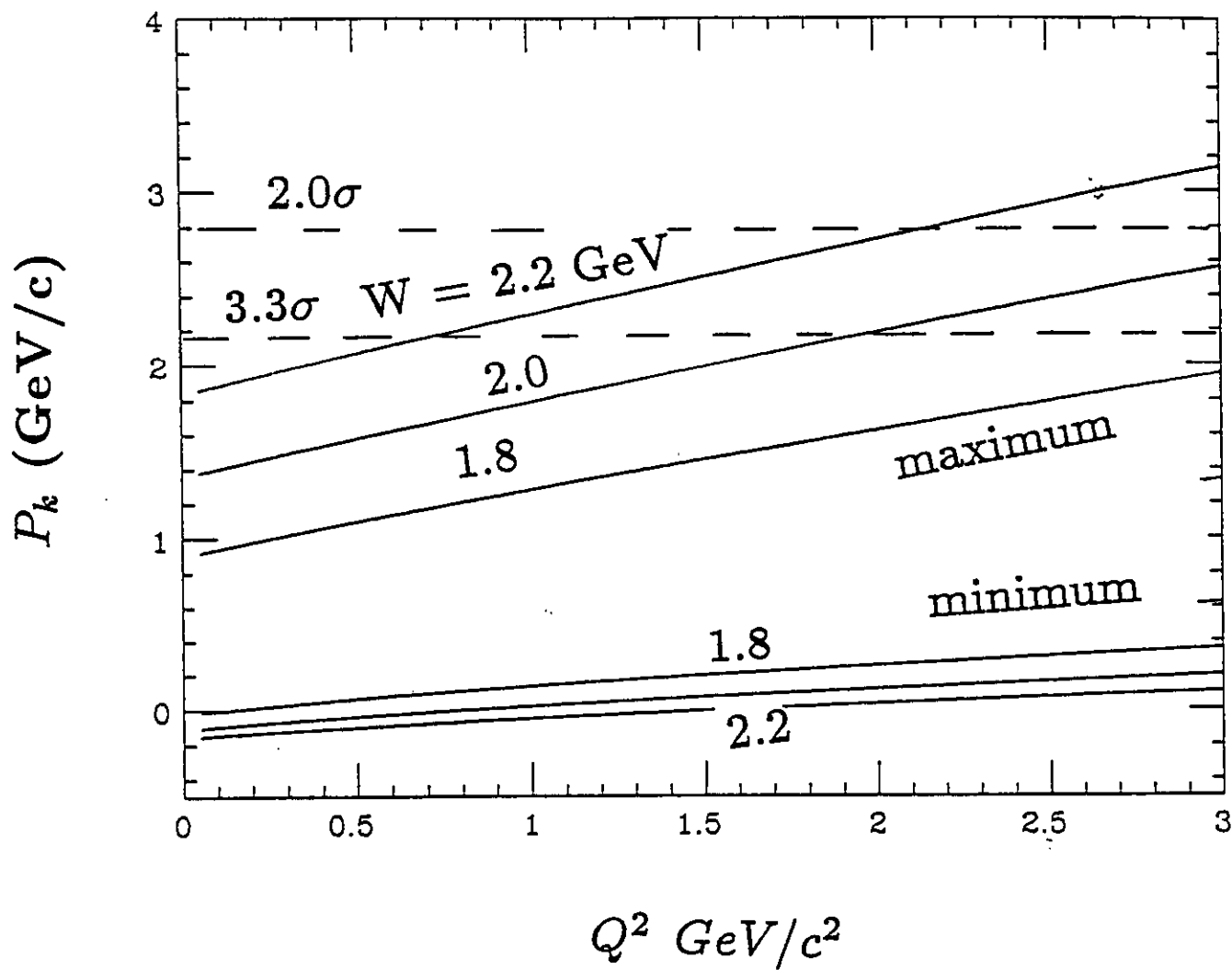
Figure 14: Maximum and minimum values of kaon laboratory momentum plotted versus Q^2. Lines correspond to different values of W.
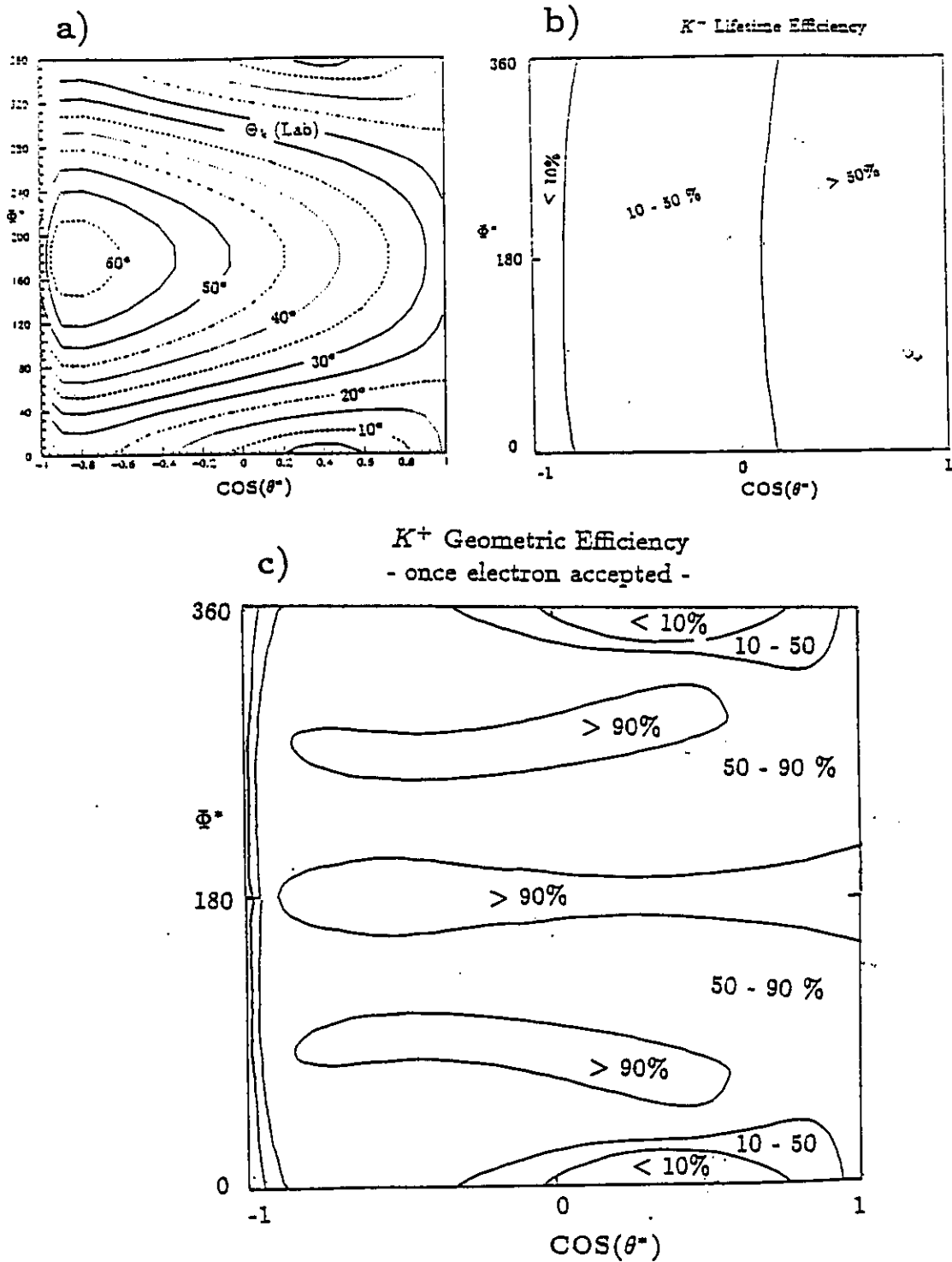
Figure 15: a) Contours of constant kaon polar angle in laboratory system (5 degree intervals) plotted versus c.m. quantities $\cos(\theta^*)$ and ϕ^*. b) Probability that track does not decay before reaching the time of flight counters; for kaons versus $\cos(\theta^*)$ and ϕ^*. c) Geometrical acceptance for kaons (assuming the electron is detected) versus $\cos(\theta^*)$ and ϕ^*.
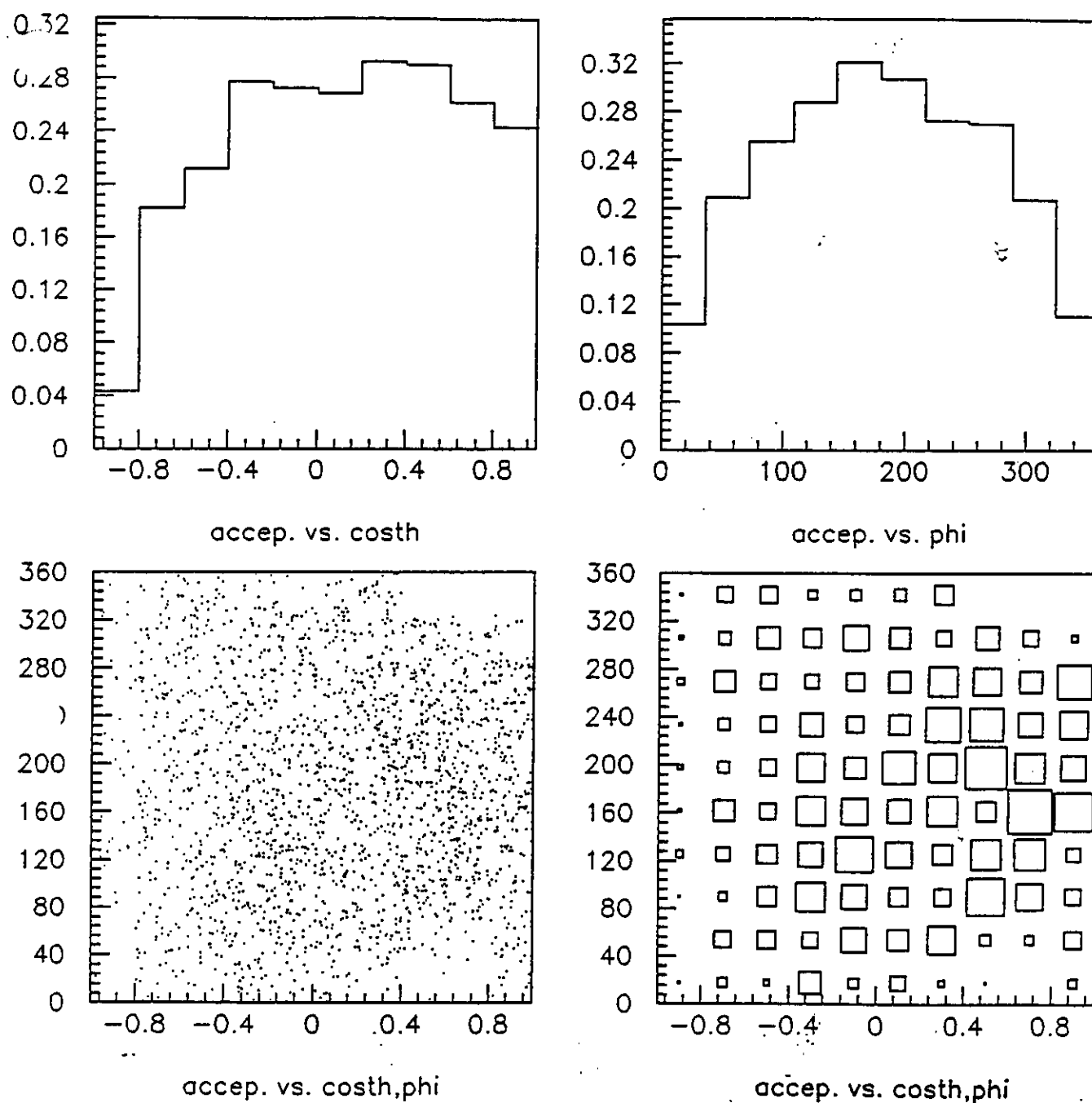
Figure 16: Overall event acceptance versus $\cos(\theta^*)$ and ϕ^* for $Q^2 = 1.0$, $W = 1.8$, $E_0 = 4.0$
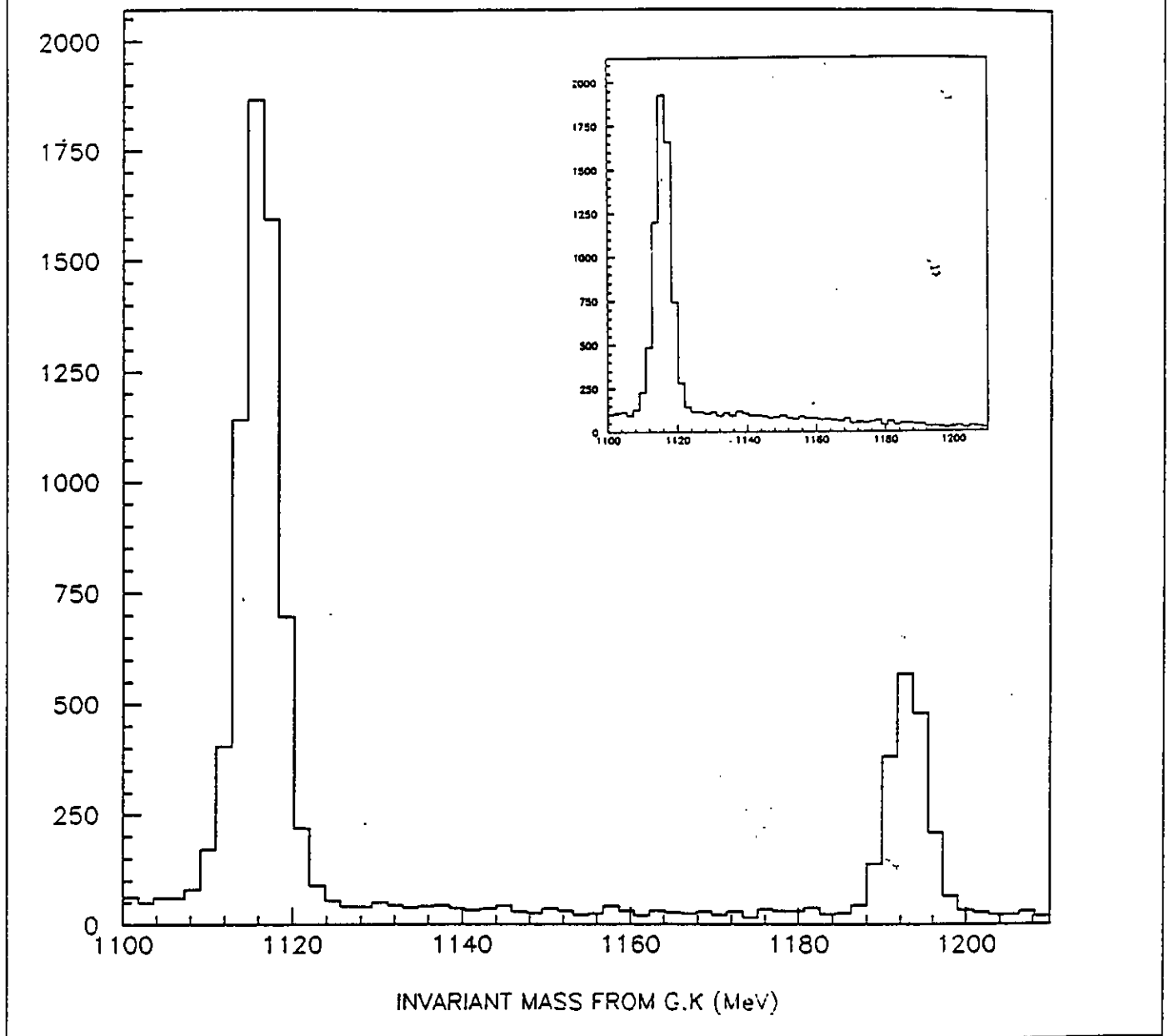
Figure 17: Missing mass recoiling against K^+. The reflection of the $\Delta_0\pi$ state where the π is misidentified as a kaon produces the smooth background shown under the Λ and Σ peaks. The figure represents a situation where the ratio of $\Delta\pi$ to ΛK is 10:1, and at a momentum, $p_k = 2.16$ GeV/c where 10% of the pions fake kaons. The separation of the Λ and Σ peaks illustrates the mass resolution of the CLAS detector. The inset shows the background condition for the case where the kaon is going forward in the hadronic center of mass.
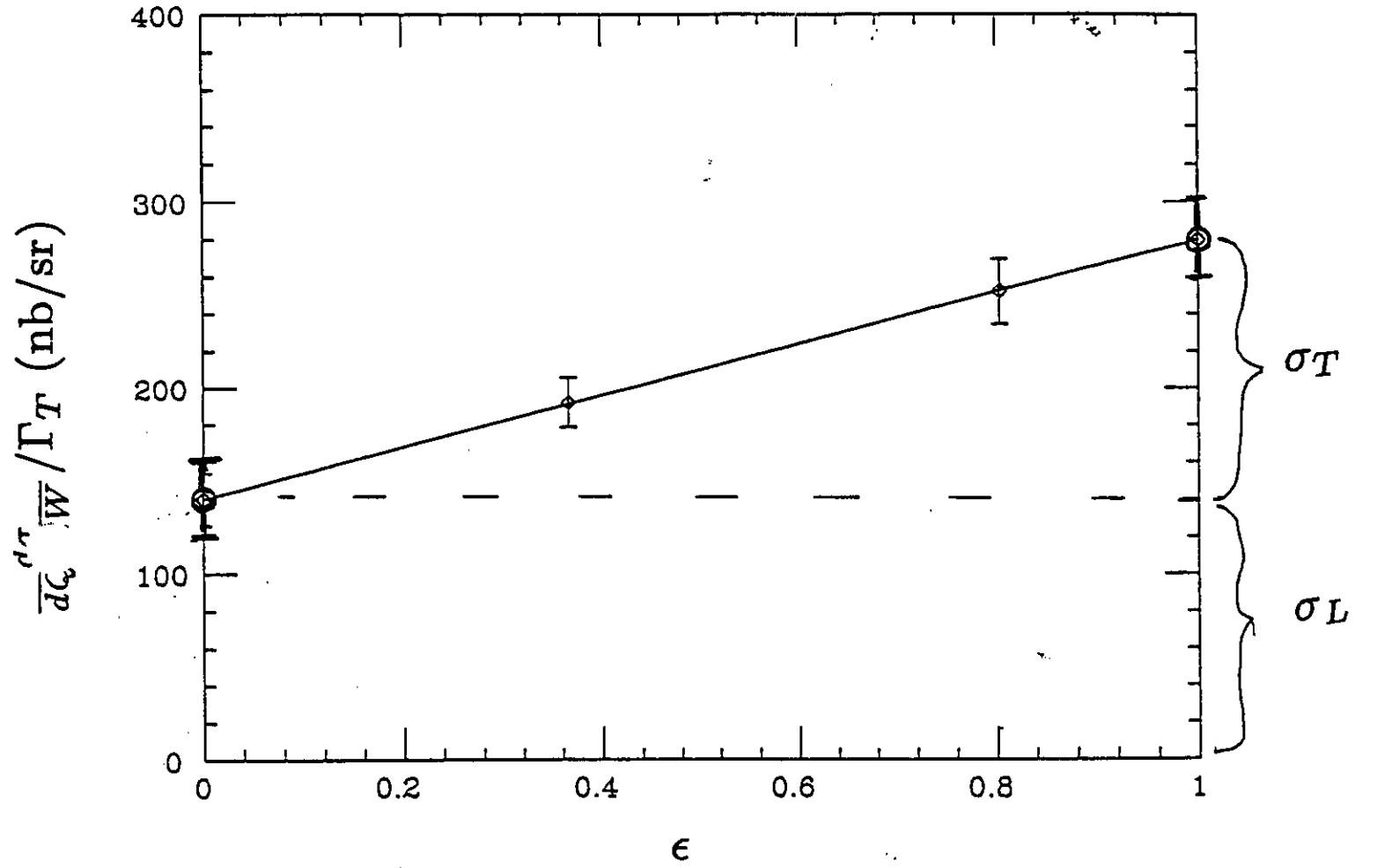
Figure 18: Differential cross section divided by the photon flux factor $,\Gamma$, plotted versus ϵ for a data point at $Q^2 =1.0$, W=1.8 GeV. Errors shown are 7%, corresponding to the size of our estimated systematic errors (see text).

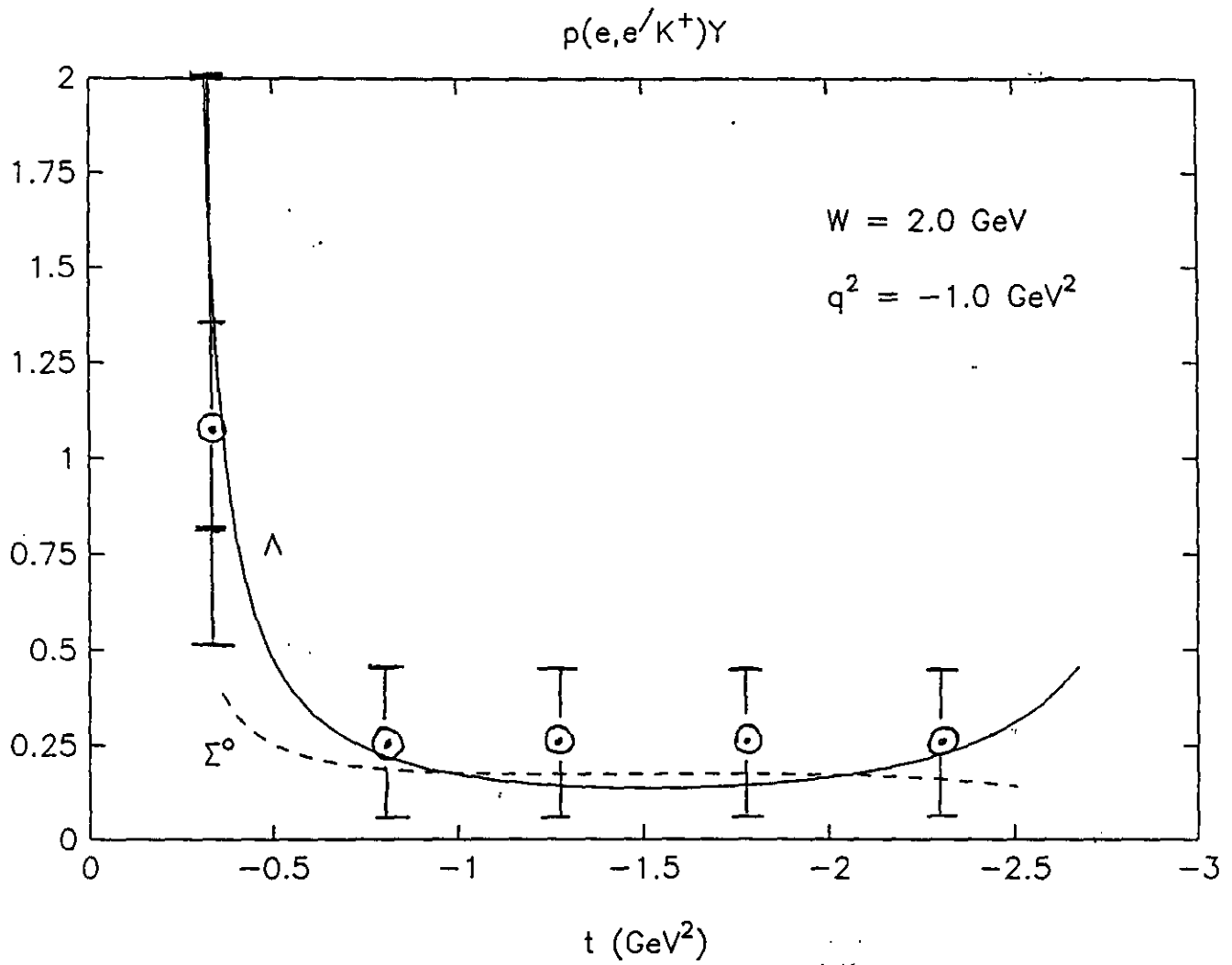Figure 19: Plot of the expected errors on $\sigma_L \,/\, \sigma_T$ plotted versus t. The data point at t_{min} is from Refernece 1; the smaller (included) error bars indicate this experiment's sensitivity. The other four data points are collected simultaneously.
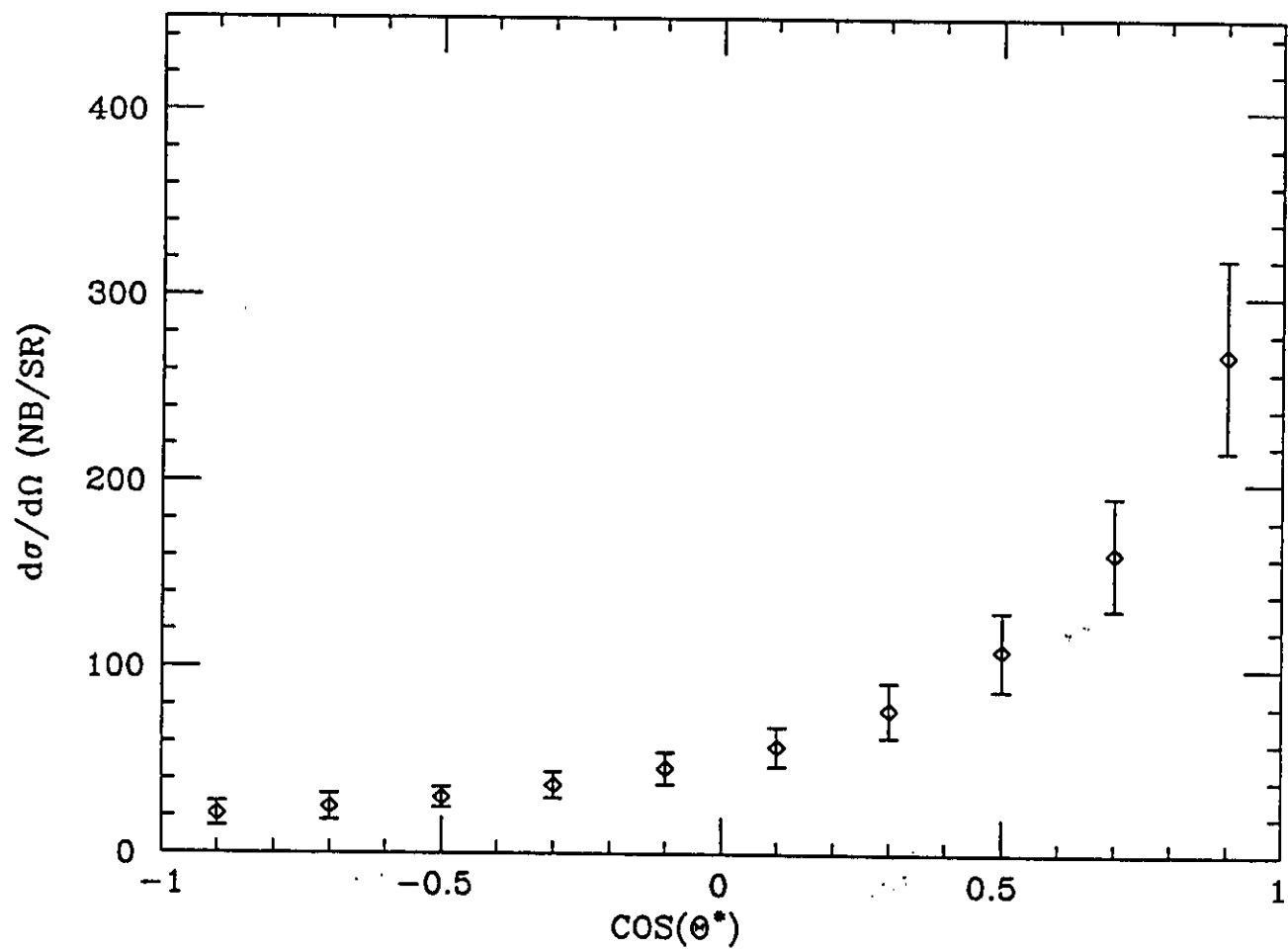
Figure 20: Plot of the expected errors on the differential cross section, plotted versus $\cos(\theta^*)$. The form of the cross section is given from a calculation by Bennhold.

Appendix : A Semirelativistic Quark Model

A. Kumar and D. S. Onley

Department of Physics, Ohio University, Athens, Ohio 45701

We use a simple quark model (Ref. [1]) for hadronic and electromagnetic interactions which is an extension of the nonrelativistic Isgur-Karl model (Ref. [2]) and is similar to the Quark Pair Creation (QPC) model of Le Yaouanc *et. al.* (Ref. [3]). The wavefunctions are obtained from the simplest form of the IK model Hamiltonian :

$$H_{IK} = \sum_i \left[\frac{\mathbf{p}_i^2}{2m_i} + m_i \right] + \frac{1}{2} K \sum_{i<j} (\mathbf{r}_i - \mathbf{r}_j)^2 \tag{1}$$

where K is flavor independent, m_i and $\mathbf{p}_i$ are the mass and momentum of the ith quark, and $\mathbf{r}_i$ is its coordinate.

Although the treatment we have used is nonrelativistic, in order to create $q\bar{q}$ pairs we need at least a quasi Dirac type description. We consider quark-antiquark production by a photon to happen analogous to electron-positron pair production using the Dirac equation. This requires that the constituent quarks be good Dirac point-like particles and, in particular, have the magnetic moment $\mu_i = (q_i\hbar)/(2m_i)$. One can take the nonrelativistic limit of this process (ignoring the small component of the Dirac wavefunction) provided we allow the nonrelativistic description to be embellished with annihilation and creation of quark-antiquark pairs. The Hamiltonian can be written in the second quantized notation as follows:

$$\frac{1}{2m} [\boldsymbol{\sigma} \cdot (\mathbf{p} - q\mathbf{A})]^2 \left[\alpha_{ps}^\dagger \alpha_{ps} + \beta_{\bar{p}\bar{s}}^\dagger \beta_{\bar{p}\bar{s}} \right] + m + (\boldsymbol{\sigma} \cdot \mathbf{p}) \left[\alpha_{ps}^\dagger \beta_{\bar{p}\bar{s}}^\dagger + \alpha_{ps} \beta_{\bar{p}\bar{s}} \right] \tag{2}$$

where q is the charge of the quark, $\mathbf{A}$ is the electromagnetic field operator, α and β refer to the quark and antiquark respectively, the subscripts p and s refer to the momentum and the spin, the bar, $\bar{p}, \bar{s}$, refers to the time-reversed states. If second quantization is not used, the above expression can be written in terms of a production operator σ_{prod}

$$\frac{1}{2m} [\boldsymbol{\sigma} \cdot (\mathbf{p} - q\mathbf{A})]^2 + (\sigma_{prod})_i \cdot (\mathbf{p}_i - q_i\mathbf{A}) + h.c \tag{3}$$

where

$$(\sigma_{prod})_i = \delta(\mathbf{r}_i - \mathbf{r}_{\bar{i}}) [(\hat{x} + i\hat{y})(\uparrow \bar{\uparrow}) - (\hat{x} - i\hat{y})(\downarrow \bar{\downarrow}) + \hat{z}(\uparrow \bar{\downarrow} + \downarrow \bar{\uparrow})](r\bar{r} + g\bar{g} + b\bar{b}) \tag{4}$$

which has the effect of laying down a pair of spin $\frac{1}{2}$ particles in the spin triplet and color singlet states. This introduces the quark antiquark pair with the appropriate vacuum quantum numbers. The bar over indicates the antiparticle coordinates and quantum numbers.

In particular, the creation/annihilation part of the Hamiltonian must be

$$H_{ca} = \left[\sum_i (\sigma_{prod})_i \cdot (\mathbf{p}_i - q_i\mathbf{A}) + h.c.\right] \qquad (5)$$

Here the non-electromagnetic production piece corresponds to the QPC term, except in that model the term has an arbitrary coupling constant; here there is no opportunity to adjust the coupling strength. The rest of the Hamiltonian describes the quarks bound in the IK-like potential wells and their ordinary electric and magnetic interactions:

$$
\begin{aligned}
H &= \sum_i \left[\frac{1}{2m_i}(\mathbf{p}_i - q_i\mathbf{A})^2 + m_i + [\mu_i\sigma_i \cdot \nabla\times\mathbf{A}]\right] \\
&+ \sum_{ij} V_{ij}^{(2)} P^{(2)} + \sum_{ijk} V_{ijk}^{(3)} P^{(3)} + H_{ca} + H_{em}
\end{aligned}
\qquad (6)
$$

H_{em} is the Hamiltonian of the free electromagnetic field.

The first term in Eq. (6) has the kinetic energy piece where $\mathbf{p}_i$ and m_i are the momentum and mass of the ith quark respectively; notice that the mass-energy has also to be included. The interaction between the quarks is represented by V_{ij} and V_{ijk}, the 2 and 3 body harmonic oscillator potentials depending only on the interquark separations. The projection operators $P^{(2)}$ and $P^{(3)}$ select out the $q\bar{q}$ and 3-q color singlet states respectively. As can be seen from H_{ca}, the photon may either directly create a $q\bar{q}$ pair in the vacuum (direct production) or couple to any of the quark lines, which then may be accompanied by the ex-nihilo creation of the $q\bar{q}$ pair in the manner of the QPC model (indirect production).

We have investigated the interaction

$$\gamma + p \rightarrow K^+ + \Lambda^0 \qquad (7)$$

in the above model. The relative momentum in the initial state defines the z axis, then since we are considering real photons, the photon polarisation vectors can be written as $\epsilon_\pm = \mp\frac{1}{\sqrt{2}}(\hat{x} \pm i\hat{y})$.

In the process (7), the $s\bar{s}$ quark pair may be created by direct production or by indirect production as defined earlier. Fig. 1 shows the $K\Lambda$ production processes diagrammatically; a set of parallel $q\bar{q}$ or $3q$ tracks indicates a bound state in the $V^{(2)}$ or $V^{(3)}$ potential. An external photon may couple to any of the quarks inside, the sum of the amplitudes is then shown as the photon line ending on a loop around the tracks. Fig. 1(a) is the direct production; the $s\bar{s}$ is created directly by the photon and the other quarks rearrange themselves to form new particles as the clusters separate. Fig. 1(b) represents the indirect production which consists of three parts depending on whether photoabsorption is by the quarks in the proton, the Λ, or the K^+. Indirect

2

production also admits all kinds of intermediate excited hadronic states which can be described in the quark model. Thus, when the photon is absorbed by any of the 3 quarks which make up the proton, it may continue as an intermediate N^* states to the point where the $s\bar{s}$ originates. Likewise the K^{*+} and the Σ^0 or Y^* can appear as intermediate states (in Fig. 1(c,d)).

Corresponding to the quark flow diagrams, we can draw several conventional Feynman diagrams (Figure 2). The diagram 1(a) gives rise to the "seagull" diagram 2(a). The indirect production graphs are shown with different intermediate states, thus 1(b) gives rise to the two graphs in 2(b), one with an intermediate proton and one with N^*. The first graphs shown in 2(b-d) are called the Born terms and, along with 2(a), contribute the major portion to the cross section. In principle all the intermediate states should be included in calculating the total cross section. At present, we have only included those low energy resonances which were thought to be significant in previous calculations (Ref. [4]). The coupling constants and form factors at the vertices in each case are given by the quark model.

The amplitudes corresponding to different initial and final spin states are calculated in the center of momentum of the γp system. The differential cross section for the process and polarisation of the Λ are then calculated.. The total amplitude for this process with just the Born terms and the Σ^0 and K^{*+} intermediate states gives a differential cross section comparable with available experimental data from threshold to 1.4 GeV. Including further intermediate states only improves the fit slightly. Figs. 3 and 4 show the angular distribution of the differential cross section at photon lab energies of 1.0 GeV and 1.2 GeV respectively as compared to available experimental data (Refs. [5],[6]). Fig. 5 shows the energy distribution at 90° angle in the center of momentum frame.

We find that kaon photoproduction is well described near threshold and in the low-energy resonance region by this model. Such energies are accessible to prospective users of CEBAF both for investigation of the elementary form of the interaction and for potential use as a probe of nuclei and hypernuclei. Aside from electromagnetic interactions, the introduction of $q\bar{q}$ production terms means that the model includes mechanisms identified with strong interactions and decays. Thus the same quark model could be used for getting information from production/decay of the mesons η, ρ and ω, as well as Y^*, N^* and Δ resonances. For interaction and propogation in nuclear matter the structure of hadrons has the potential of being changed to some extent, and this too might be understood in terms of a constituent quark model.

References

[*] Supported by U S Department of Energy Grant DE-FG02-87ER40370

[1] A. Kumar and D. Onley, Bull. Am. Phys. Soc. 37, 1319 (1992).

[2] N. Isgur and G. Karl, Phys. Rev. D18, 4187 (1978).

[3] A. Le Yaouanc, L.Oliver, O. Pène and J.-C. Raynal, Phys. Rev. D8, 2223 (1973)

[4] R. A. Adelseck, C. Bennhold and L. E. Wright, Phys. Rev. C32, 1681 (1985)

[5] R. L. Anderson, Phys. Rev. Lett. 9, 131 (1962)
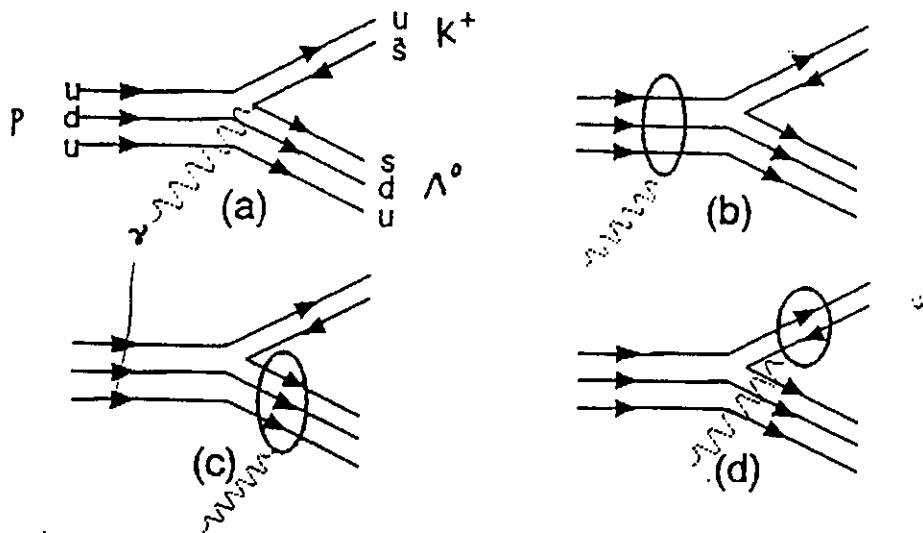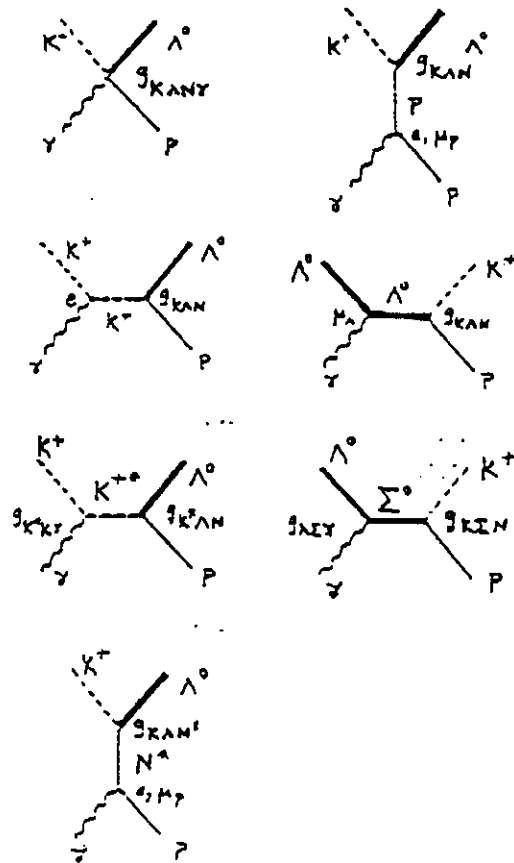
[6] C. W. Peck, Phys. Rev. 135, B830 (1964)

Figure 1

Figure 2

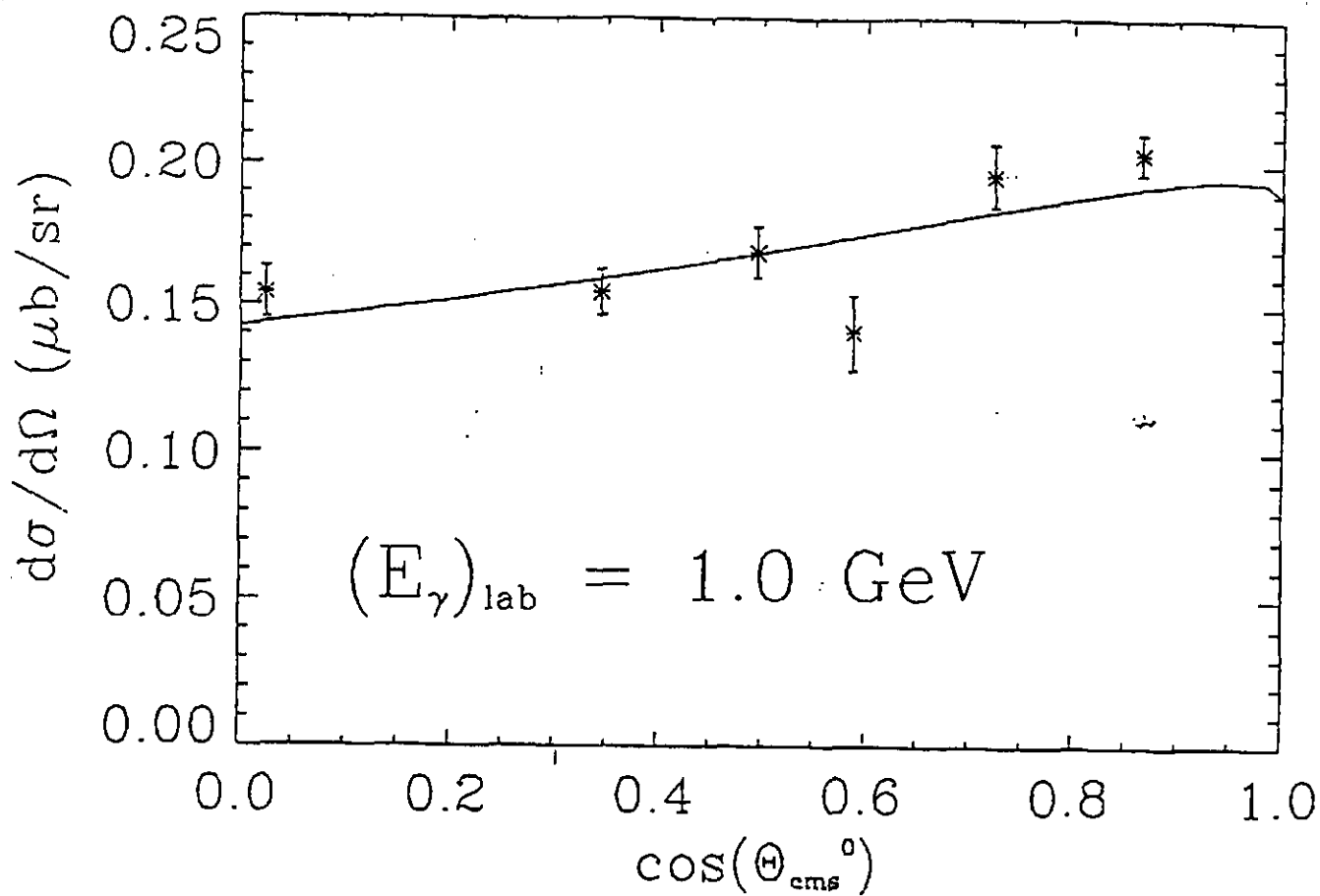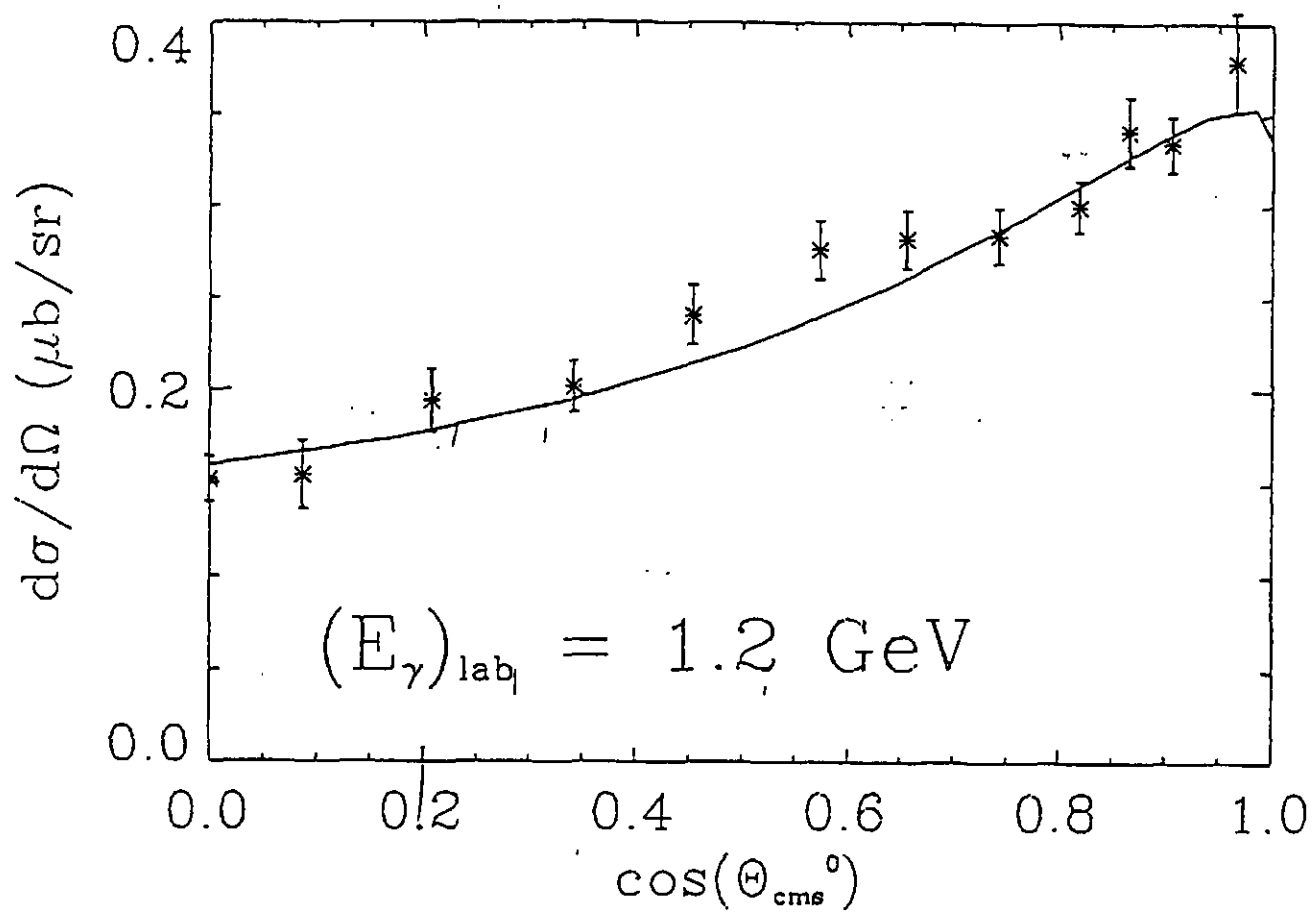$(E_\gamma)_{lab} = 1.0$ GeV

Figure 3

$(E_\gamma)_{lab} = 1.2$ GeV

Figure 4

Figure 5